In: Image Processing
Editor: Vítor Hugo Carvalho

ISBN 978-1-62081-844-2


*Chapter 1*

# IMAGE PROCESSING: CHARACTERISTICS AND APPLICATIONS IN TEXTILE INDUSTRY AND BIOMEDICINE

***Vítor Carvalho[1,*], Filomena Soares[1], Nuno Gonçalves[1], Ana Ferraz[1], Rosa Vasconcelos[2] and Michael Belsley[3]***
[1]Department of Industrial Electronics,
[2]Department of Textile Engineering,
[3]Department of Physics, Minho University, Guimarães, Portugal

## ABSTRACT

This chapter presents the main characteristics and functionalities of two systems based on image processing techniques applied to Textile Industry and Biomedicine.

In Textile Industry we used image processing to determine yarn mass parameters as well as yarn production characteristics. A low cost solution based on a web-pc camera plus the optics of a low cost analogue microscope and a software tool based on IMAQ Vision from LabVIEW was designed. Several tests were performed and compared with other methodologies of yarn parameterization validating the proposed solution. With the results one can support that this can be an alternative solution to the traditional yarn testers, with several advantages (among others, low cost, weight, volume, easy maintenance and reduced hardware).

In Biomedicine we used image processing to develop a system capable of determining human blood types for emergency situations and so with a fast response. With this system it is possible to obtain a reliable result in less than 2 minutes, allowing the administration of the specific blood type of the individual in the first transfusion, as well as avoiding human errors witch several times can result in fatal consequences. As in the previous system, this solution is based on a web-pc camera plus and a software tool based on IMAQ Vision from LabVIEW, and so of low cost. Several tests were performed in order to validate the proposed methodology being obtained reliable results.

* E-mail address: vcarvalho@dei.uminho.pt.

## INTRODUCTION

In Textile Industry, image processing is employed to characterize yarn diameter, hairiness, and mass as well as yarn production characteristics (fibers twist orientation, folded yarn twist step, folded yarn twist orientation and the existence of single, non-folded yarn, or multiple cables, folded yarn) [1-15]. The correct evaluation of yarns is of utmost importance for the textile industry as the quality of the final product relies directly on the yarn. Currently, there is commercial equipment capable of testing yarns; one of the most used is the Uster Tester 5. Despite their contribution to the yarn's characterization, these devices have some drawbacks, such as, high cost, large size and considerable weight in addition to a limited resolution and accuracy in determining mass parameters. Technological solutions based on Image Processing (IP), are characterized by high reliability and efficiency and can remove all the drawbacks identified in traditional solutions as well as introducing the determination of new parameters not yet determined by the traditional and commercial equipment (as example, the distinction between hairiness resulting from loop or protruding fibers and the yarn production characteristics). The acquisition system consists of a low cost CMOS camera coupled to a low cost analogue microscope in order to obtain the necessary optical amplification and reducing the camera resolution requirements. To analyze the acquired images an image processing application was developed using the IMAQ Vision software from LabVIEW from National Instruments.

In Biomedicine image processing is applied to develop a methodology to determine human blood types in emergency situations.

Determining the blood type of an individual is an essential procedure before administering a blood transfusion, avoiding injury and blood incompatibilities. Thus, the preceding blood test, even in case of medical emergency, is of upmost importance, allowing the correct administration of the blood type of the receiver in the first unit of blood transfusion. However, although two of the manual tests used in laboratory, the plate and the tube test, allow the analysis in a short time interval, which is suitable for emergency situations, they require travel to the lab and the intervention of a technician, thereby increasing the time spent and the possibility of human error. Given that human errors in the procedure of manual tests, in reading or interpreting the results, can lead to fatal consequences for patients, being one of the significant causes of fatal blood transfusions, it is important to automate the testing, the reading and the interpretation of results.

The developed system is based on the plate test for determining blood types and in custom developed software using the IMAQ Vision software from LabVIEW from National Instruments, using image processing techniques. The plate test consists of four different mixtures of one drop of blood and one drop of the specific reagent, being the result interpreted according to the occurrence or not of agglutination. The agglutination means that a reaction has occurred between the antibody and the cells, indicating the presence of the appropriate antigen. The combination of the occurrence of agglutination, or non-occurrence, determines the blood type of the individual. Thus, the developed software allows, through image processing techniques, to detect the existence of agglutination and consequently the blood type of an individual eliminating human error and in a short interval of time, to be used in emergency situations [10, 11, 16-23].

It is the author's believe that the proposed solutions based on image processing techniques enable a correct and complete yarn parameterization, that come across Textile Industry requirements, as well an accurate human blood type determination.

## IMAGE PROCESSING AS A TOOL TO PARAMETERIZE YARN MASS PARAMETERS

This section presents the framework, the textile parameters theoretical configuration, the system development and the experimental results.

### Framework

The correct and accurate evaluation of yarns is a subject of major importance to the Textile Industry, as the final fabric quality depends directly on the yarn quality. To undertake these yarn tests several companies have developed specific equipment. The Tester 5 from Uster is important for its relevant contribution to the development of quantitative yarn characterization. However, these yarn testers have a significant cost, require a considerable area for their installation and present limited resolution and precision in the evaluation of certain yarn parameters. As a result, many yarn producers do not have their own yarn testers and, instead, choose to subcontract dedicated testing laboratories for yarn quality determination. This process is time consuming and eliminates the possibility of acting in useful time during yarn production, reducing efficiency.

To overcome these drawbacks, new equipment, entitled YSQ (Yarn System Quality) [9] was developed. The YSQ measures yarn diameter, yarn hairiness and yarn irregularity based on optical and capacitive sensors. Moreover, it integrates an external module to obtain yarn production characteristics, based on image processing (IP). At present, in the Textile Industry there is no available commercial equipment or known prototypes to automatically obtain these characteristics. Instead, they are obtained manually by human ocular inspection or by using an analogue microscope, being the results susceptible to errors [24, 25].

The high precision levels of parameterization performed by the YSQ, together with its low cost and high portability make it a reliable and efficient solution for the Industry.

Furthermore, and after studying the image processing possibilities in the production characteristics module of the YSQ, we started considering to specify the traditional yarn mass parameters as technological solutions based on IP, as they are characterized by high reliability and efficiency and can present some advantages over the traditional methods (low cost, small size and weight, reduced hardware, reliability and possibility of high resolution).

IP (Image Processing) based applications have been used in the textile field since 1964 [4] although they have not yet been converted to viable quality control methods [6].

Due to its influence on the quality of textiles, yarn hairiness is considered to be one of the most significant parameters. In textile industry the equipment used to measure the hairiness are based on photoelectric methods, like the Shirley's apparatus and the Uster Tester 3 devices. [7] Several algorithms are currently under development to characterize the yarn hairiness with IP. The method proposed by [8], measures the real length of the protruding

fibers from the yarn core, as well as, their number in order to quantify hairiness. In [2], it is introduced a new method to measure hairiness, based on the assumption that the hairs close and parallel to the yarn core would be a better indicator of hairiness, proposing then a new parameter: Hair Area Index. This concept measures the area covered by hairs and is divided by the area of the yarn core to obtain a dimensionless quantity. Nevertheless, it is still necessary to develop algorithms to detect and characterize loop fibers length and to clearly distinguish between protruding fibers and loop fibers when they are interlaced.

Another important parameter is the yarn diameter, since it is used to predict fabric structural parameters such as width, cover factor, porosity and fabric comfort [26]. The characterization of yarn diameter with IP can also be achieved with algorithms already applied to the extraction of yarn core [7, 8]. But, algorithms to measure the exact length of yarn irregularities (thin places, thick places and neps) [12] need to be developed. The characterization of yarn mass can be inferred from the yarn diameter, depending, among other parameters, on the yarn fiber density and porosity.

Besides the YSQ, this section presents a new solution to automatically characterize the mass parameters of yarn based on IP.

## Textile Parameters Theoretical Considerations

This section describes the typical configuration of a yarn, the definition of faults, hairiness and the most important yarn production characteristics [9, 25, 26].

### *Yarn Configuration, Faults and Hairiness*

The most important parameters used to specify yarn quality are linear density, structural features and fibre content. An example of yarn configuration is shown in Figure 1.

As Figure 1 suggests there is a direct relationship between the variation of yarn mass and the yarn diameter. Thus the calculation of the diameter can be obtained by the theoretical correlation d(mm) = 0.037sqrt(Tex) [26], where Tex is the mass of the yarn in one kilometer of length (g/km) – yarn linear mass. This relation allows the possibility of determining yarn irregularity based on yarn diameter measurements.

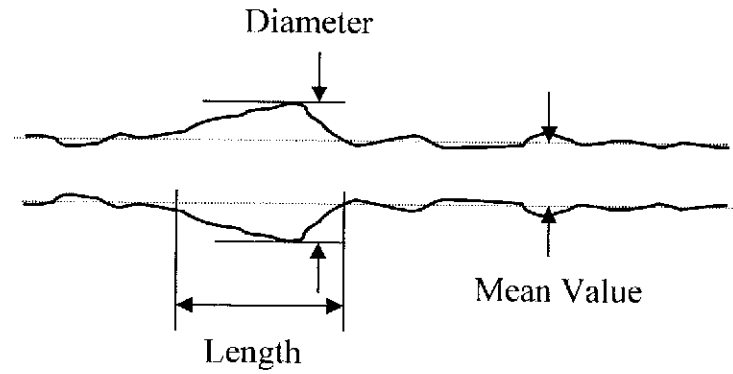


Figure 1. Example of yarn configuration.

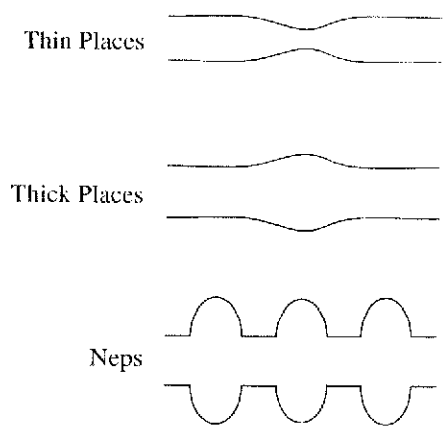


Figure 2. Types of yarn faults.

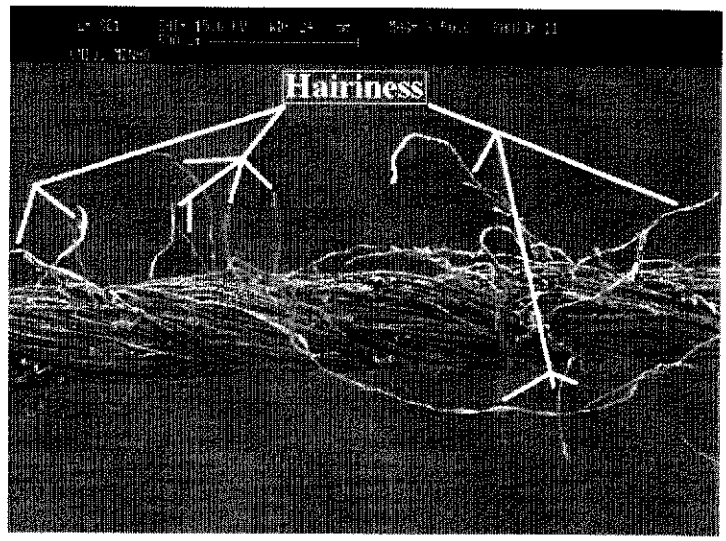


Figure 3. Identification of yarn hairiness in an electron microscope picture.

The number of yarn faults and yarn mass measurements enables a quality rating of the products tested. There are three kinds of yarn faults, classified as (Figure 2): thin places - a decrease in the mass during a short length (4 mm); thick places - an increase in the mass, usually less than 100 % of the sensitivity, and lasting more than 4 mm; neps - huge amount of yarn mass (equal or superior to 100 % of sensitivity) in a short length (typically from 1 mm to 4 mm).

Apart from faults, another important feature which greatly influences the appearance of fabrics is the level of yarn hairiness. Hairiness is the result of released fibres over the strand. Figure 3 presents an example of hairiness [9].

The hairiness coefficient (H) specifies the length of hairs in a meter of yarn. The measurements of yarn hairiness, mass and diameter, allow the determination of several statistical parameters which are relevant when characterizing yarn quality and, subsequently, the fabrics.

### *Yarn Production Characteristics*

Four important production characteristics of commercial yarns are the fiber's twist orientation, the number of cables (folded yarns and non-folded yarns), the folded yarn twist step and the folded yarn twist orientation [9]. The two final production characteristics mentioned are only obtained when dealing with folded yarns.

Figure 4 identifies the four described production characteristics using as an example an electron microscope image of a 4.2 g/km cotton yarn. It is a folded yarn as two separate cables are clearly visible. The folded yarn twist step (d) is 0.3334 mm, with an orientation clockwise and a fiber twist orientation opposite (anti-clockwise) to the folded yarn direction.

This section describes experimental setup used in the image acquisition, as well as the yarn production characteristics software application, the diameter and imperfections software application, and the yarn hairiness determination software application.

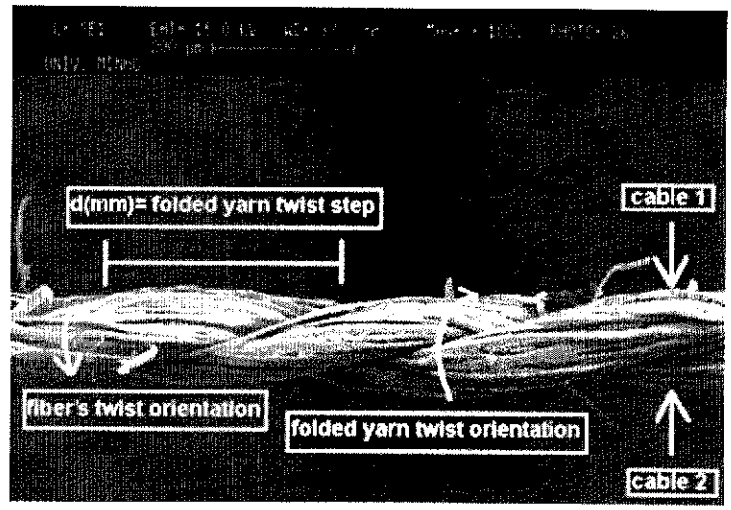


Figure 4. Identification of the yarn production characteristics in an electron microscope picture.

## System Development

### *Experimental Setup – Acquisition Image Processing Systems*

The experimental set-up for obtaining yarn images consists of a low cost analogue microscope coupled to a common web CMOS camera. The microscope provides sufficient amplification and image detail, while there are no special requirements regarding the camera resolution. Figure 5 shows a flowchart of the designed system.

The analogue microscope used is the Biolux Al from Bresser [27], which has the following main characteristics:

- 2 oculars of 5X and 16X;
- 3 objectives of 4X, 10X and 40X;
- a Barlow lens of 2X;
- Led illumination.

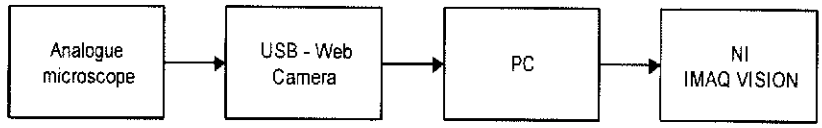


Figure 5. Designed system flowchart.

For the images described in this work, the 5X ocular lens was used, together with the 4X objective and the 2X Barlow lens, leading to an overall optical amplification of 40X (5x4x2). This amplification level was sufficient to obtain reliable results for yarns with a wide range of linear masses. However, if necessary, alternative magnifications can be used within the limits of the available set of lenses. The USB Web Camera employed is the Deluxe model from Hercules [28], which has the following characteristics:

- Photosensitive element: 1/4" CMOS sensor;
- Resolution: 640x480 pixels
- Video mode: VGA;
- Color format: 24 bit – true color.

The web camera was placed at the exit plane of the microscope ocular, capturing the analogue image produced by the microscope. With an optical amplification of 40X, a sensor resolution of 640x480 pixels is adequate to correctly evaluate the yarn production characteristics.

In order to obtain higher contrasts for the yarn geometry relief, the illuminated yarn surface must be as close as possible to a monochromatic light source. As the white led illumination available with the microscope emits a wide range of wavelengths, we decided to use an external yellow light source, which is somewhat closer to an ideal monochromatic light source. Figure 6 illustrate two different images acquired when using the white light source from the microscope and the external yellow light source respectively.

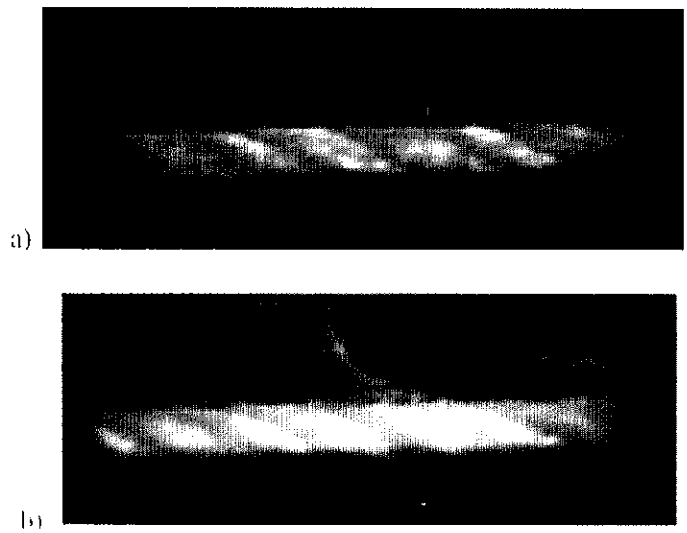


Figure 6. Yarn cross-section images resulting from white (a) and yellow (b) illumination.

As shown in these images, with the yellow light source, the contrast between the yarn zones with higher relief is more accentuated. The regions which correspond to the most accentuated twist areas or yarn areas closer to the light source (Figure 1- 6 b)), are more clearly distinguished.

To analyze the acquired images an image processing application was developed using the IMAQ Vision software from LabVIEW from National Instruments.

### *Image Calibration*

In order to calibrate the images, an image of an object with known dimensions was acquired (Figure 7).

In Figure 7 the real world distance between the lines is 1 mm, while, in the acquired image corresponds to 73 pixels.

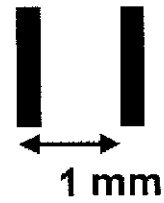


Figure 7. Image used for calibrating the system with real world measurements.

### *Yarn Production Characteristics Software Application*

In this section we demonstrate the influence of the techniques employed, using two examples of the different yarns studied during the development of the system. The methodologies employed were validated through the common commercial range of 100% cotton linear mass yarns.

The raw images were processed with the following functions from the IMAQ Vision software in order to determine the production characteristics of a given yarn:

1. Contrasts adjust – expressed as a value between 1 and 89. The median value of 45 corresponds to a neutral setting, no contrast alteration, while higher values produce greater contrast. As it was intended to increase the contrast of the relief transition zones, the maximum value (89) was selected [10, 11].
2. Gamma Adjust – this specifies the value considered in Gamma Correction. Higher coefficients are associated with weaker intensity corrections. As it was intended to reduce as much as possible the intensity correction, in order to separate the relief transition zones, the highest value (10) was used [10,11].

Figure 9 presents the results obtained on the original image (Figure 8) after adjusting the contrast and gamma, to their highest values.

As a result of the steps 1 and 2, all pixels with intensities lower than those acquired in the transition zones have been effectively set to zero intensity.

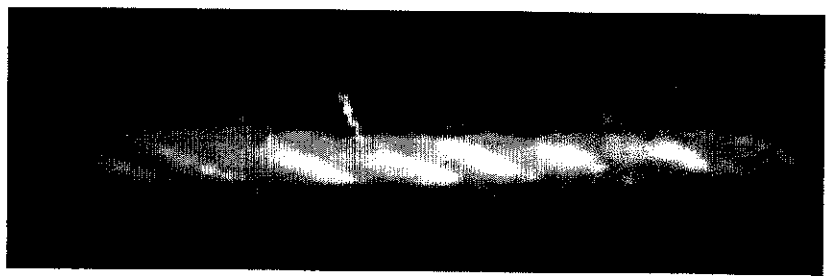

Figure 8. Original image as acquired by the web camera.

Figure 9. The resulting image after setting the contrast to 89 and the gamma adjust to 10.

Figure 10. Image resulting from the application of the Removal of the Luminance Plane over the HSL to the image of Figure 9.

3. To simplify the binary image conversion process, it is desirable to homogenize the colour distributions in the image presented in Figure 9. This can be accomplished using the "Removal of the Luminance Plane over the HSL (Hue Saturation Luminance) Color Space" tool [10, 11].

Figure 10 presents the resulting image after applying the Removal of the Luminance Plane on the image in Figure 9.

This step converted the three different tonalities presented in Figure 9, namely, red, yellow and white, to dark gray, light gray and white, reducing significantly the color intensity spectrum of the original image.

4. Auto Threshold: Inter Variance – the Threshold function consists of segmenting an image into two regions, namely, a "particle" region and a background region, setting to "1" all the image pixels with a gray level equal to or above a given gray level threshold (threshold interval) and setting to "0" all the other pixels. This process is used to isolate certain areas in an image. In order to select the threshold interval

automatically, the Auto Threshold Interclass Variance tool was employed. This method determines an optimal threshold level by maximizing the between-class variation with respect to the threshold. The threshold value is the pixel value $k$ (gray level chosen as the threshold) at which eq. 1 (variance) is maximized [10, 11].

$$\sigma_B^{\,2}(k) = \frac{\left[\sum_{i=0}^{N-1} ip(i) \times \sum_{i=0}^{k} p(i) - \sum_{i=0}^{k} ip(i)\right]^2}{\sum_{i=0}^{k} p(i)\left[1 - \sum_{i=0}^{k} p(i)\right]} \tag{1}$$

where, $N$ is the number of gray levels in the image. The numbers $p(i)$, are the occurrence probability of a given gray level $i$, namely

$$p(i) = \frac{h(i)}{\sum_{i=0}^{N-1} h(i)} \tag{2}$$

Here, $h(i)$, represents the total number of pixels with a given gray level value $i$.

Figure 11 shows the resulting image after applying the Auto Inter Variance function to Figure 10. As expected, the application of the binary algorithm has isolated all the pixels with the relevant information (pixels different from black color, in this case).

Figure 11. Image resulting from the application of the Auto Threshold: Inter Variance, to the image of Figure 10.

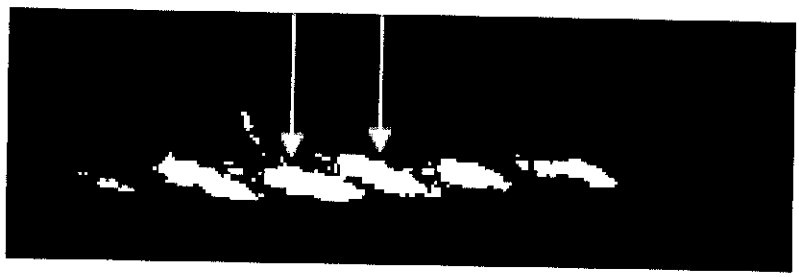

Figure 12. Image resulting from the application of the Hole Filling function to the image in Figure 11.

5. Hole Filling – this function fills the holes within continuous bright parts of the image in order to homogenize the binary images [10, 11].

The application of the Hole Filling function to Figure 11 is illustrated in Figure 12; three holes identified in Figure 11 by the white arrows have been filled.

6. Erosion – this function eliminates isolated pixels in the background and erodes the contour of particles according to a defined structuring element. This structuring element is a 2D binary mask, which defines the size and effect of the neighborhood on each pixel, controlling the effect of the binary morphological function on the shape and boundary of a particle. In this case we considered a 3x3 matrix containing values of 1. For a certain pixel P0, the structuring element is centered on P0. If the coefficient of the structuring element is equal to 1, the masked pixels are referred as Pi [10, 11]:

   a. If the value of one pixel Pi, is equal to 0, then P0 is set to 0, otherwise P0 is set to 1.
   b. If the logical AND of Pi is equal to 1, then P0 is set to 1, otherwise P0 is set to 0.

This function eliminates unwanted particles and avoids the possibility of object aggregation. Figure 13 presents the application of the Erosion function described above to the image of Figure 12.

As a result, the particles are now well separated. This is especially important for those particles that were particularly close to one another (identified with white arrows in Figure 12), which could easily been considered as one particle, rather than two. In addition, almost all the other irrelevant information has been also removed.

7. Convex Hull – this function *closes* particles in order to allow measurements even when the particle contour is discontinuous. It calculates a convex envelope around each particle, closing it [10, 11]. This function was used to allow use to carry out the necessary particle measurements.

As Figure 14 shows, the application of the Convex Hull function drastically reduces the discontinuity of the particles observed in Figure 13.

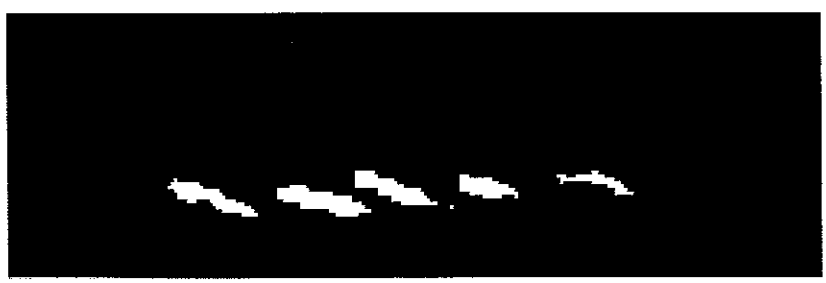

Figure 14. Image resulting from the application of the Erosion function to the image of Figure 12.

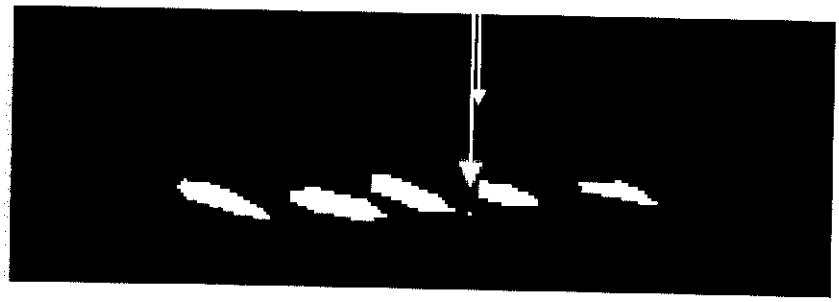

Figure 14. Image resulting from the application of the Convex Hull function to the image of Figure 13.

8. Small Objects Removal – This step is based on successive applications of the erosion tool followed by dilatation. This results in the elimination of the small particles and smoothing of the larger particle boundaries. Since erosion and dilatation are complementary transformations, for large particles, this operation does not significantly change the area or the shape as the borders removed by the erosion function are restored by the dilatation function [10, 11].

The result of a single application of this operation is shown in Figure 15. The small particles identified by the white arrow in Figure 12, have been removed in Figure 13, maintaining the other particles essentially unaltered. However, as this algorithm is for general use and, as in some cases the undesired small particles are slightly larger than the particles eliminated by a single iteration, a double iteration of this operation was used. In this example, the first particle on the right was eliminated (Figure 16). However, the loss of this particle is of little consequence as the number of particles remaining is enough to determine the desired parameters.

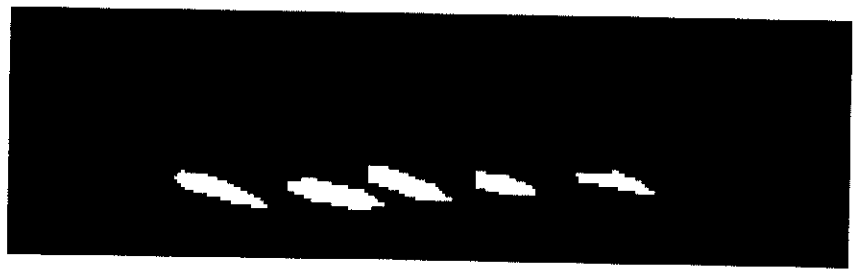

Figure 15. Image resulting from the first application of the Small Objects Removal function to the image of Figure 14.

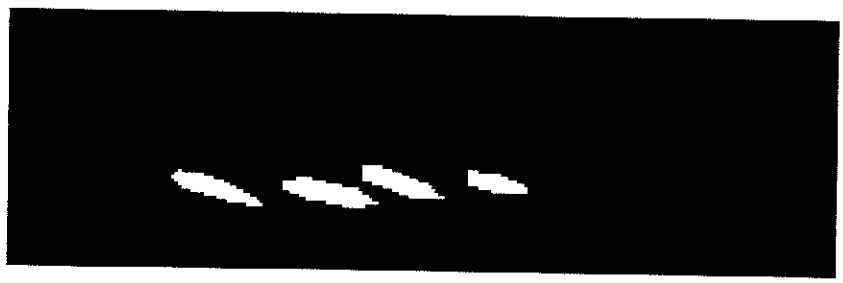

Figure 16. Image resulting from the second application of the Small Objects Removal function.

9. Particle Analysis - This function is used to perform several types of measurements over the particles of a binary image. Specifically in this study, the following parameters were employed [10, 11]:

   a. First horizontal pixel – the horizontal coordinate of the first particle pixel.
   b. Determination of Orientation: the angle ($\alpha$) of the line that passes through the particle Centre of Mass corresponding to the lowest moment of inertia (eq. 3). The orientation angle is measured counter clockwise using the horizontal axis as a reference, over a range between 0° and 180° (190 ° is reported as a 10° angle).

$$\alpha(^\circ) = \frac{1}{2}\arctan\left(\frac{2\sum xy}{\sum yy - \sum xx}\right) \tag{3}$$

where, $x$ and $y$ are, respectively, the horizontal and vertical pixel coordinates of the line corresponding to the lowest moment of inertia.

   c. Area: area of the particle

Upon carrying out the above imaging processing procedures, it is possible to apply the following steps to determine the desired yarn production characteristics:

- Folded yarn twist step, which is the average of the horizontal pixel distance between particles: This parameter is only relevant when the yarn contains more than one cable (folded yarn), i.e. when at least two particles have been identified.
- Folded yarn twist orientation: This parameter is determined by the orientation angle for each particle:
  - If the orientation angle lies between 90° and 180°, then the twist orientation is anti-clockwise.
  - If the orientation angle lies between 0° and 90°, then the twist orientation is identified as being in the clockwise direction. Of course, the yarn must have at least two cables (folded yarn) in order to make it possible to determine the folded yarn twist orientation.
- Number of cables (folded or non-folded yarn):
  - If only one particle is identified then the yarn is identified as a single cable (non folded yarn).
  - If the number of particles is greater than one, then the yarn is identified as possessing multiple cables (folded yarn).
- Fibers twist orientation: two possible situations may occur:

- When the yarn is constituted by more than one cable (folded yarn), the fibers twist orientation is opposite to the folded yarn twist orientation. This is a universal situation in Textile Industry, done to avoid untwisting of the fibers over the yarns [3, 4].
- When considering a single cable yarn (non folded yarn) a new function is called.

In order to obtain the fibers twist orientation in non folded yarns, the following algorithm was used:

1. Removal of the intensity plane of the HIS (Hue, Saturation and Intensity) Color encoding scheme: In single cable yarns, a large region of the yarn should have a high intensity level [10, 11]. With the removal of the intensity plane, the intensity distribution over the yarn becomes more homogeneous.

Figure 17 presents the original yarn image and Figure 18 shows the result after the removal of the intensity plane which produces a much more uniform intensity distribution.

Figure 17. Image used for the development of the twist orientation for a single cable yarn.

Figure 18. Image resulting from the application of the intensity plane of the HIS color scheme.

2. Convolution – Highlight Details: A convolution is an algorithm that recalculates the value of a pixel based on its own value and the pixel values of its neighbors weighted by the coefficients of a convolution kernel. The convolution kernel defines how the associated filter alters the pixel values in a grayscale image. It is a 2D structure whose coefficients define how the filtered value at each pixel is computed. Considering several iterative tests, a 7x7 kernel containing 60 in the centre and -1 at all the other positions was used [10, 11]. Two iterations were performed in order to obtain a good definition of the high relief fibers (closer to the light source) which constitute the yarn.

Figure 19 presents the result of the convolution after the first iteration; in Figure 20 is the result after the second iteration. The image of figure is used 16 as a reference.

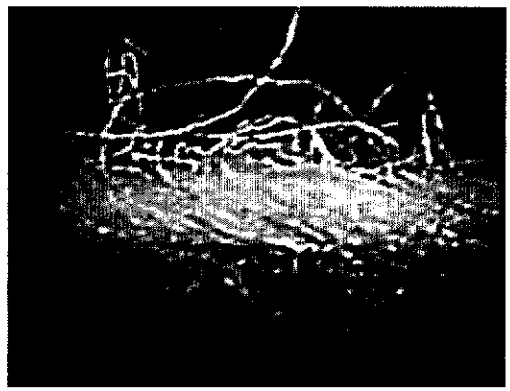

Figure 19. Image resulting from the application of the Convolution function to the image of Figure 18.

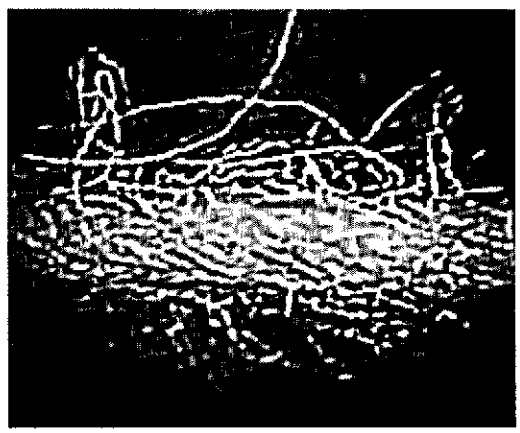

Figure 20. Image resulting from the second application of the Convolution function.

It was observed that only two iterations are needed to greatly increase the visibility of the external yarn fibers.

4. Auto Threshold-Moments: The threshold moments method is based on the assumption that the observed image is a blurred version of the theoretical binary

original. The blurring that is produced from the acquisition process, caused by electronic noise or a slight imperfection in the optics, is assumed not to alter significantly either the average or the variance of the pixels intensity distribution. This function recalculates a theoretical binary image. The $k^{th}$ moment $m$ of an image is calculated by eq. 4 [10, 11].

$$m_k = \frac{1}{n}\sum_{i=0}^{i=N-1} i^k h(i) \tag{4}$$

where, $n$ is the total number of pixels in the image.

The Auto Threshold – Moments were considered to isolate the white details obtained in the figure 18.

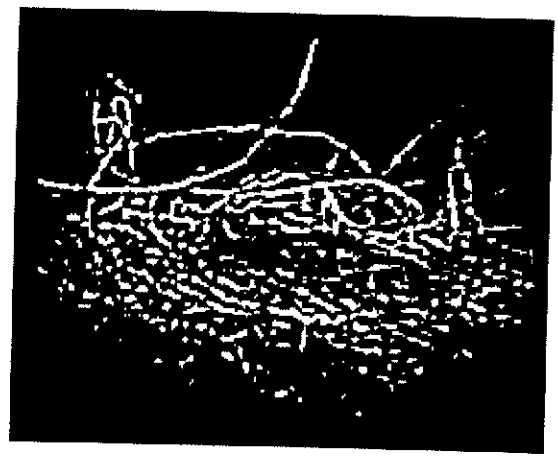

Figure 21. Image resulting from the application of the Auto Threshold – Moments function to the image of Figure 20.

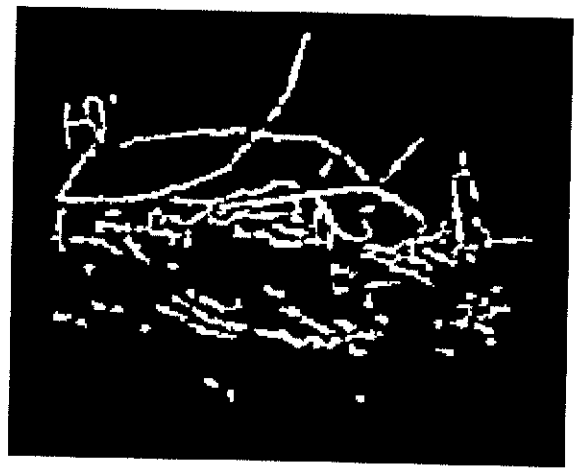

Figure 22. Image resulting from the application of the Small Objects Removal function to the image in Figure 21.

Figure 21 presents the results obtained after the application of the Auto Threshold – Moments function on the image of Figure 20, showing an excellent isolation of the image details.

4. Small Objects Removal: This option was used to remove all the small particles present in Figure 21[10, 11].

Figure 22 presents the results obtained upon applying the Small Objects Removal tool to the image of Figure 21.

5. Labeling: This function assigns a different gray level value to each particle in the image. The result is not a binary image, but a labeled image which uses a number of gray level values equal to the number of particles in the image, plus the gray level zero assigned to the background area. This function identifies particles using either connectivity-4 or connectivity-8 criteria. The connectivity criteria define the neighborhood a given pixel. For connectivity-4, only adjacent pixels in the horizontal and vertical directions are considered neighbors, for connectivity-8, all adjacent pixels are considered neighbors. For the cases studied, connectivity-4 produced better results [10, 11]. This reduces the influence of the neighborhood pixels and subsequently produces a more differentiated gray level labeling of the particles corresponding to fibers which protrude from the yarn core.

Figure 23 presents the results of the Labeling function used on the image of Figure 22. As observed, the binary image has been separated into several objects, identified by different colors and where the protruding particles are displayed with a lower grey level.

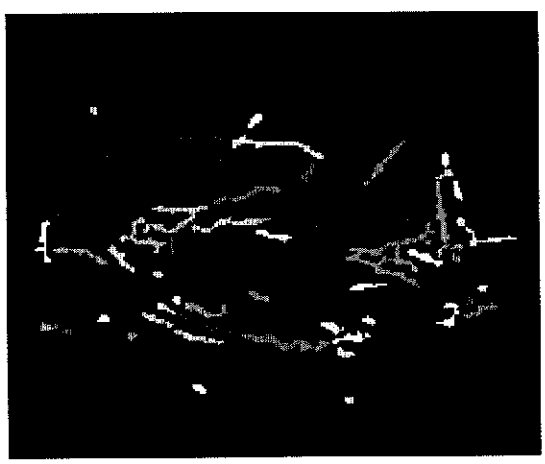

Figure 23. Image resulting from the application of the Labeling function to the image of Figure 22.

6. Exponential: This function decreases brightness and increases contrast in bright regions of an image, decreasing contrast in dark regions [10, 11]. Here, this step was important to eliminate fibers protruding from the yarn core.

Figure 24. Image resulting from the application of the Exponential function to the image of Figure 23.

Figure 25. Image resulting from the application of the Convex Hull function to the image in Figure 24.

Figure 26. Image resulting from the application of the Particle Area Filter function to the image of Figure 1-25.

Figure 24 presents the result of applying the exponential function to Figure 23. Besides removing the protruding particles, the labeling color in the remaining particles has changed, due to the alterations in brightness.

7. Convex Hull – As previously, this function was used to permit the necessary particle measurements [10, 11].

After the application of the convex hull tool to the image of Figure 24, the image in Figure 25 was obtained. As intended, the level of discontinuity of each particle has been reduced.

Particle Filter: The goal of this function is to remove all the particles with reduced areas. Considering multiple case studies, it was concluded that for the optical amplification used, removing all particles with an area inferior to 34 pixels (threshold) allows proper results [10, 11].

Figure 26 presents the use of the particle area filter in the previous image.

8. Particle Analysis – Orientation: Measuring the orientation angle of each particle enables the determination of the twist orientation [10, 11]. The considered strategy calculates the average orientation of all particles in the image. Then, as in section B:

   a. If the average angle orientation lies between 90º and 180º, then the twist orientation is anti-clockwise.
   b. Conversely if the orientation angle within the interval from 0º to 90º, then the twist orientation is clockwise.

### *Diameter and Imperfections Software Application*

This section describes the methodology used for measuring the diameter, for calculating of the hairiness coefficient and the detection of imperfections in the yarn, through image processing techniques.

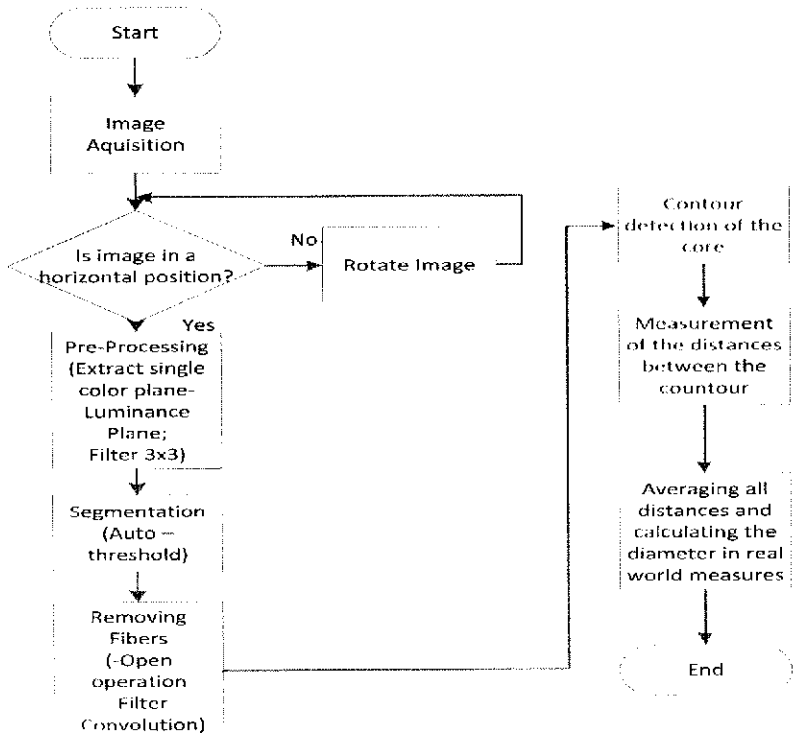


Figure 27. Diameter determination block diagram.

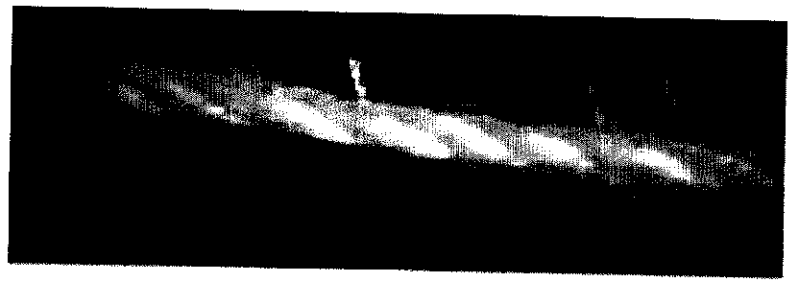

Figure 28.Original sample image acquired.

Figure 29. The resulting image after yarn rotating.

Figure 27 represents the block diagram of the algorithm used to determine the diameter by image processing techniques. The algorithm summarizes the application of various techniques of image processing that allows obtaining, as final result, the contours of the yarn core, excluding, all hairiness around the core. The diameter calculation is made through the detection of all the edges along a set of parallel searching lines. Once all edges are detected, the distance is calculated between the pairs of edges detected by all the search lines. The diameter is obtained by, the average of all the distances calculated. Once obtained the diameter, the yarn mass is easily acquired through the theoretical correlation between mass and diameter, presented previously. Figure 28 presents the image-based sample of the yarn captured by the image acquisition system. In the following, the sequence of functions used to obtain the yarn diameter is explained and their output is presented.

1. Function Rotate - If the yarn is not in the horizontal position, this function allows to rotate until the yarn is in the horizontal position [10, 11], as shown in Figure 29
2. Extract Single Color Plane, specify the luminance Plane over the HSL (Hue, Saturation and Luminance) - This function has the objective to homogenize the proximal colour patterns in order to simplify the binary image [10, 11] (Figure 30).
3. Filter nth order - The type of filter used was a zero order filter with a 3x3 matrix. With this type of filter it is possible to smooth the image and erode brighter objects, without changing the structure of the yarn [10, 11], Figure 31. This operation is highly relevant when the yarn has a large number of hairiness around the core.
4. Auto Threshold (cluster method) – This function is used to segment the image in two regions, a particle region and the background region. Threshold function converts the image to a binary image, with pixel values of 0 or 1. The clustering method is based on the following condition:

$$\frac{\mu_1+\mu_2}{2} = k \quad (5)$$

where $\mu_1$ is the mean of all pixels values that lie between 0 and k, and $\mu_2$ is the mean of all the pixel values between k+1 and 255. The option for look for the brighter objects was used to simplify the detection of the contours of the yarn in the following steps [10, 11]. This approach is possible because the yarn is mainly made up of brighter pixels. Figure 32 shows the result of the Auto Threshold function applied to Figure 31.

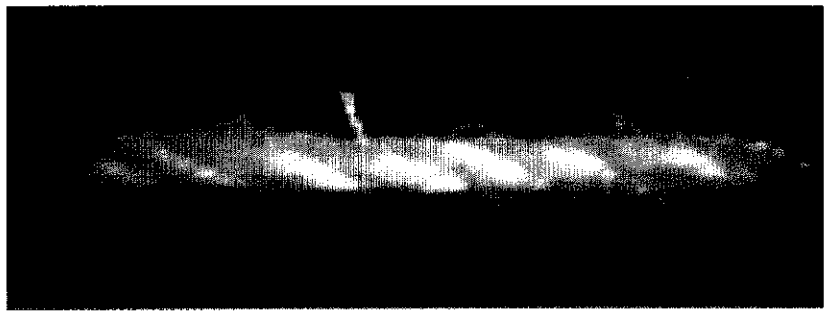

Figure 30. Image resulting after the removal of the luminance plane on the image of Figure 29.

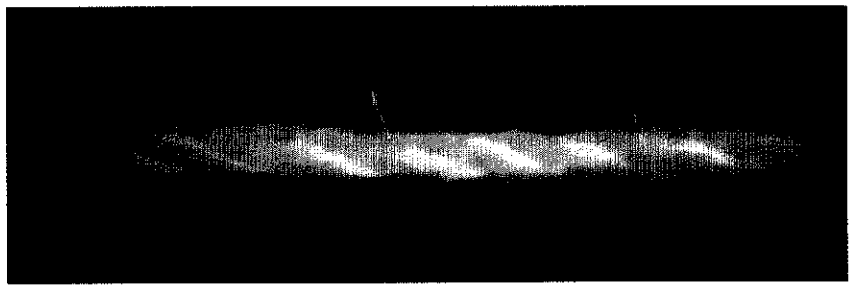

Figure 31. The resulting image from the application of the Filter to Figure 30.

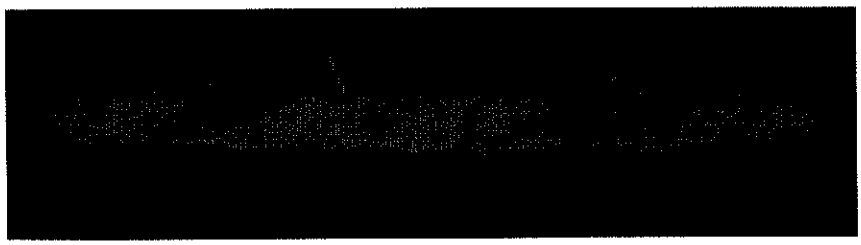

Figure 32. The resulting image from the application of the Auto threshold in Figure 31.

4. Remove particle – This function eliminates particles resistant to a specified number of 3 x 3 erosions. Five times was the number of erosion necessary in this function, to remove all small particles [10, 11], as presented in Figure 33.

6. Open - The open function consists of the operation of erosion followed by the dilation, it fills tiny holes and smoothes boundaries [10, 11] as shown in Figure 34. The value of the structuring element used was 1, using the following kernel [4, 5]:

$$\begin{bmatrix} 1 & 1 & 1 \\ 1 & 1 & 1 \\ 1 & 1 & 1 \end{bmatrix}$$

In comparison to all morphological operators, the open function showed minor changes to the yarn structure. This is an important factor to ensure greater accuracy in measuring the diameter.

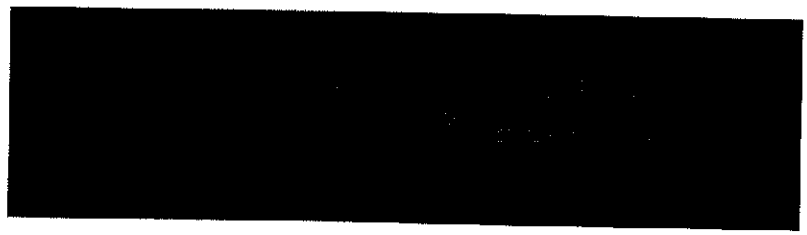

Figure 33. Image resulting after the application of the function remove particle to Figure 32.

Figure 34. Image resulting from the application of the open function to Figure 33.

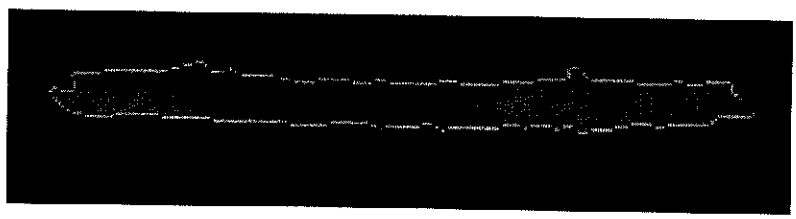

Figure 35. The resulting image after the application of the convolution function to Figure 34.

For example, when using the erosion or close function, they cause an increase or decrease in the yarn structure, which would influence the measurement of the diameter.

7. Convolute - This function allows recalculating the value of a pixel based on its own value as well as the pixel values of its neighbors weighted by the coefficients of a convolution kernel. The Laplacian convolution filter, a second-order derivate, was

used to extract the contour of objects and outline details. Figure 35, with the following kernel [10, 11]:

$$\begin{bmatrix} 0 & -1 & 0 \\ -1 & 5 & -1 \\ 0 & -1 & 0 \end{bmatrix}$$

8. Canny edge detection – This function uses a pixel value at any point along the pixel profile to define the edge strength at that point. To locate an edge point, several scans of the pixel profile are performed, pixel by pixel from the beginning to the end [10, 11], as shown in Figure 36.

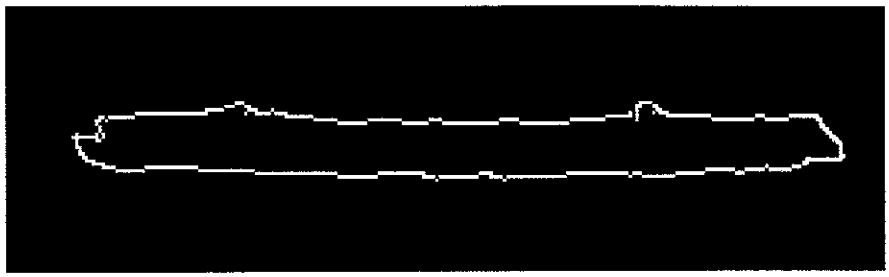

Figure 36. Image resulting from the application of the Canny edge detection.

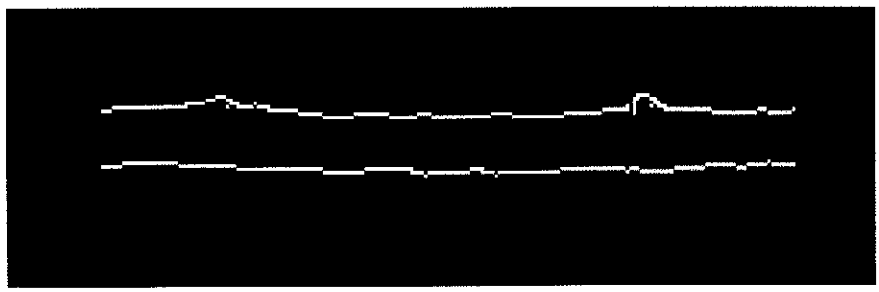

Figure 37. Image resulting from the application of a and logical between the rectangles mask and Figure 36.

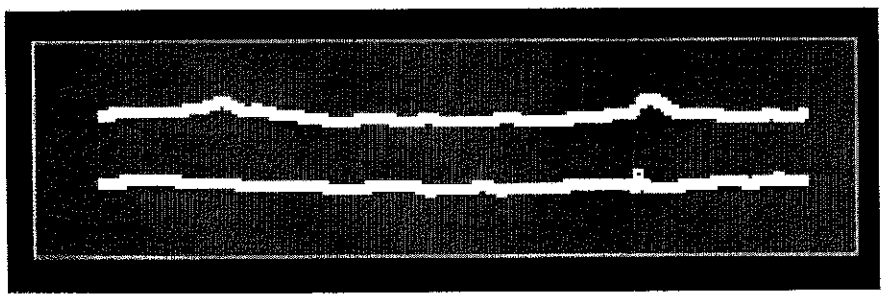

Figure 38. Final image to measure the diameter from the application the clamp vertical max function to Figure 37.

At this point it was essential eliminating the borders of the yarn, to reduce the error on measuring the distance between the edges of the yarn. For this, it was used the function *Particle analysis report*, that provides the coordinates of the center of mass of the object, which allow us to apply two rectangle mask based on these coordinates.

An *and* logical between the two rectangles masks and Figure 36 was performed resulting the image in Figure 37.

9. Clamp vertical max - This function allows finding all edges along a set of parallel searching lines, in a region of interest. The diameter is calculated by the average of the distance measured between the pair of edges detected by the searching lines. Figure 38 presents the final result.

Figure 39 presents the another image-based sample captured by the image acquisition system and Figure 40 the result after the application of the sequence of functions presented in Figure 38. With the yarn diameter and due to the correlation between the mass and the diameter, thick places, thin places and neps can be analyzed by comparing the distances measured along the yarn with the average diameter. Figure 41 shows the algorithm applied. After obtaining all measured distances in an array, it's calculated the reference values for the thin places, thick places and neps. It's considered a thin place if the current value of the array is below 50% of the average diameter, as the thick places are considered if the current value is above 40% of the average diameter.

Figure 39. Original sample image acquired.

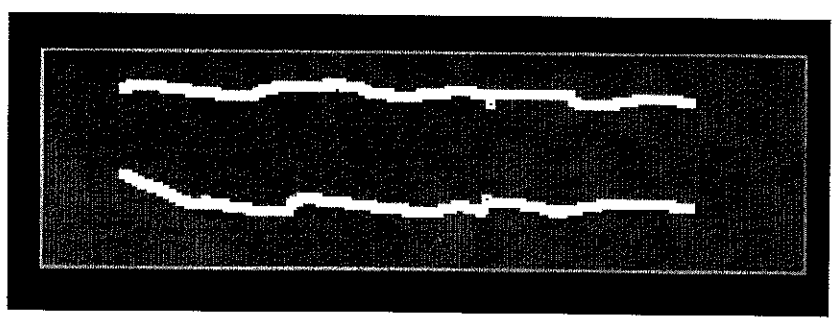

Figure 40. Image resultant from the application of the algorithm to Figure 39.

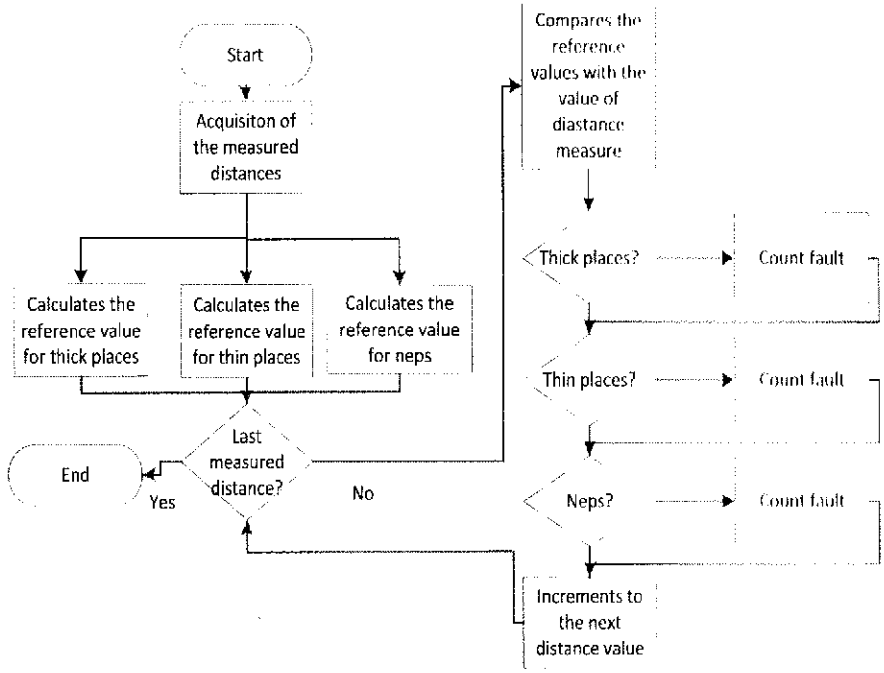


Figure 41. Algorithm used to detect yarn faults.

Finally the neps are contemplated for values above 100% of the average diameter. To avoid single values the current value it's always compared to the previous value, and they have to match, otherwise it's not considered as a fault.

### *Yarn Hairiness Determination Software Application*

In this study, spatial pre-processing techniques, as well as segmentation and spatial filtering techniques were used to isolate the yarn core and to highlight and quantify the protruding and loop fibers from the original image. In order to isolate the protruding and loop fibers from the yarn, logical operators were used between the image with the highlight fibers and the yarn core. Figure 42 presents the algorithm implemented.

Figure 43 shows the sample base yarn image where the image processing techniques were applied.

In the following the functions used to obtain yarn hairiness are explained and their output presented. The sample images were first converted to grayscale, Figure 44.

1. Function Rotate - If the yarn is not in the horizontal position, this function allows to rotate it until it is in the right position [10, 11], as shown in Figure 45.
2. Inverse – this function inverts the pixel intensities of an image to compute its negative [10, 11]. This operation allowed highlighting white and grey details over large areas of black pixels, Figure 46.
3. Equalize – This function redistributes the pixel values of an image to linearize the accumulated histogram [10, 11]. This function was used with the range between 200 to 230 in order to field the sample yarn with black pixels, Figure 47.

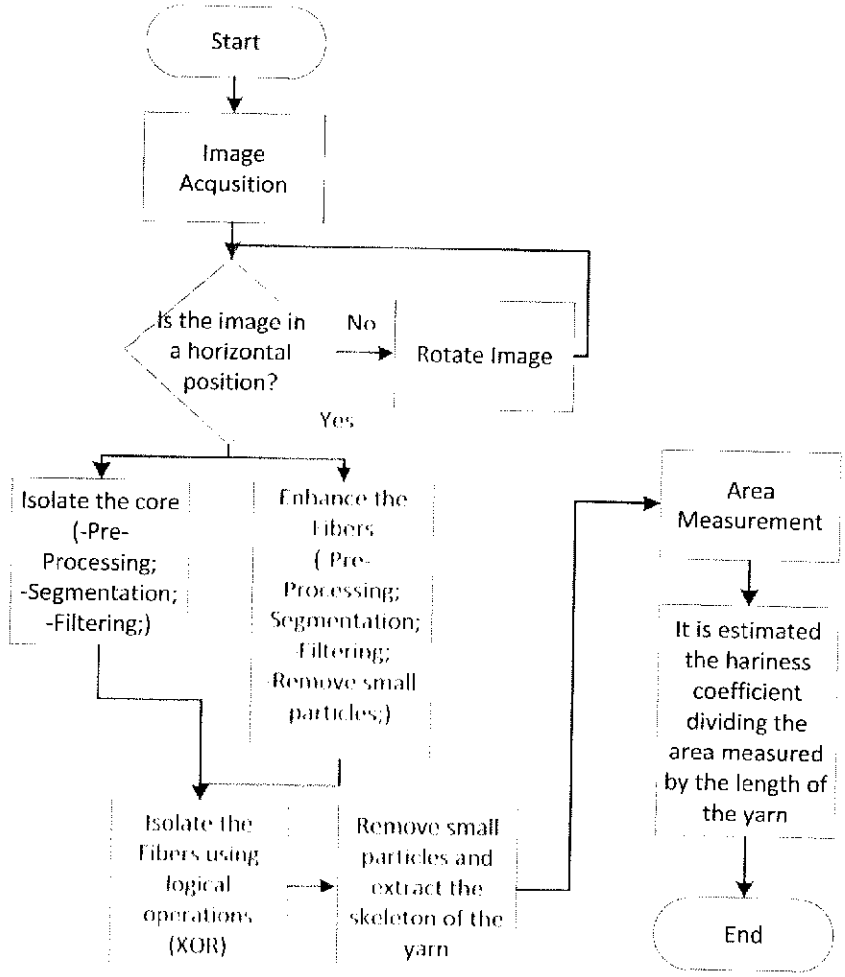


Figure 42. Algorithm used to measure the yarn hairiness index.

Figure 43. Original sample image acquired.

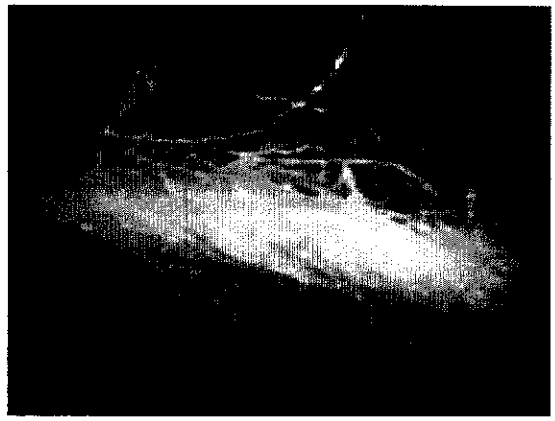

Figure 44. The resulting image in grayscale.

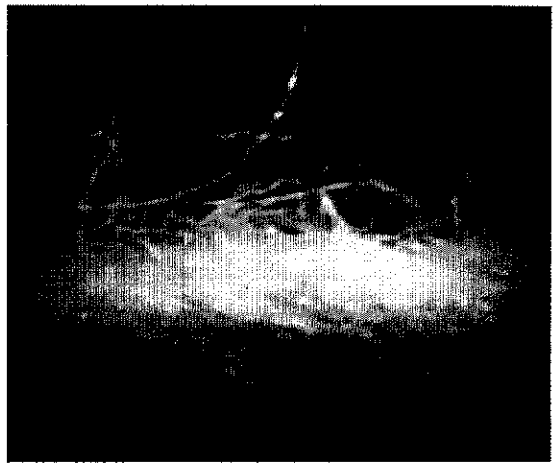

Figure 45. Image resultant after rotating.

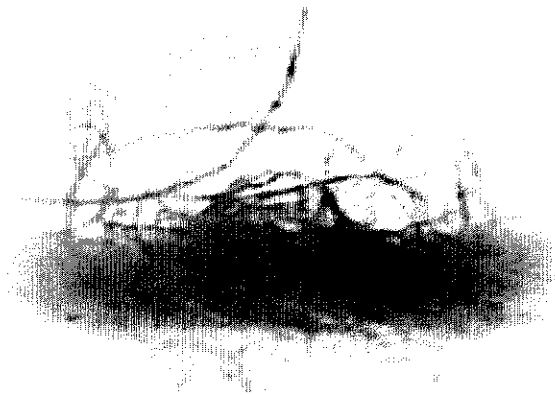

Figure 46. Resultant image from the application of the inverse function in Figure 45.

Figure 47. Image resultant after the equalize function in Figure 46.

4. Auto Threshold - This function is used to segment the image in two regions, a particle region and a background region, Figure 48; limits between 0 and 1, as well as the option for look to the darkest objects were used.
5. Filter nth order - This function was used to apply a filter of nth order to eliminate the fibers, as presented in Figure 49. By trial and error, a kernel mask 7x7 with N=4 was used due to the good results obtained [10, 11].

Figure 48. Image resultant from the application of the Auto threshold function in Figure 47.

Figure 49. Resultant image after the application of the filter in Figure 48.

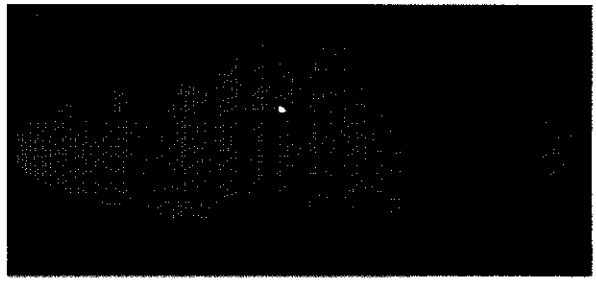

Figure 50. Image resultant from the application of the remove particle function in Figure 49.

6. Remove particle – This function eliminates particles resistant to a specified number of 3 x 3 erosions. Five times was the number of erosion necessary in this function, to remove all small particles [10, 11], as presented in Figure 50

## Algorithm to Measure the Hairiness Coefficient

This section describes the algorithm used to enhance the yarn, in particular to highlight the loop and protruding fibers, by removing the background and all unwanted particles.

In the following, the functions used to highlight the fibers are explained and the results presented. The first three functions described in the previous section were used with the same purpose.

1. Convolute - This function allows recalculating the value of a pixel based on its own value and the pixel values of its neighbours weighted by the coefficients of a convolution kernel. It was used a Laplace filter to detect points of discontinuity [10, 11] with the following kernel:

$$\begin{matrix} 0 & -1 & 0 \\ -1 & 5 & -1 \\ 0 & -1 & 0 \end{matrix}$$

Figure 51 shows the result of the convolution applied.

Figure 51. Resultant image after the application of the convolution function in Figure 47.

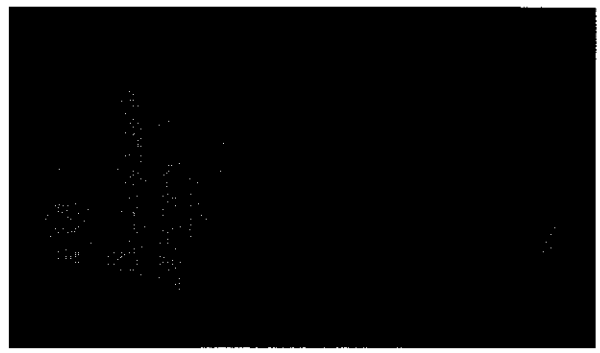

Figure 52. Image resultant from the application of threshold and small particles removal functions in Figure 51.

Figure 53. Resultant image after the logical operation and small objects removal function applied.

The final step involves the functions threshold and the removed particle, also described in the previous section, Figure 52.

2. The next step was to perform a logical exclusive or (XOR) between the Figure 50 and Figure 52 to isolate the fibers. A small objects removal was used to eliminate some remaining particles of the logical operation as shown in Figure 53.

In the following it is described the functions that allowed the measurement of the hairiness coefficient.

3. Skeleton - calculates the skeletons of the particles within an image or the lines delineating the zones of influence of the objects it applies a succession of thinning's until the width of each particle becomes equal to one pixel [10, 11]. The structuring element used was the skeleton L with the following kernel:

0 ? 1
0 1 1
0 ? 1

The resulting image is presented in Figure 54.

Once the fibers are isolated, the borders of the yarn must be eliminated to avoid its influence in the measurement of the hairiness. This was accomplished by using a two rectangles (200x15) mask with the filling value of 255 pixel and with the coordinates of the borders of the yarn, Figure 55.

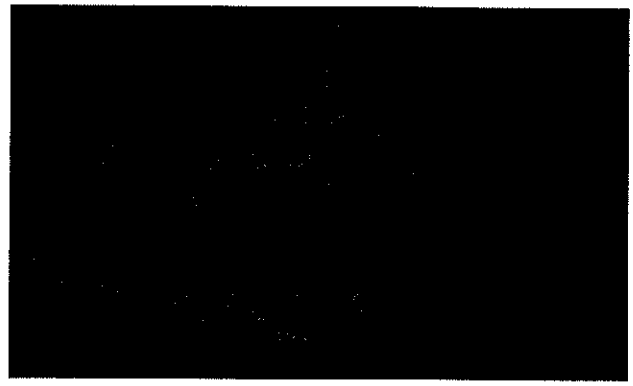

Figure 54. Image resultant from the application of the skeleton function in Figure 53.

Figure 55. Two rectangles mask used to eliminate the borders.

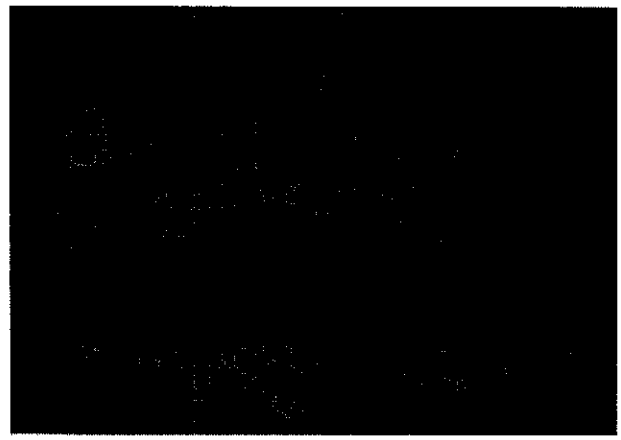

Figure 56. Resultant image from the logical operation between Figure 55 and Figure 54.

An *and* logical operation was performed in Figure 54 to eliminate the borders, Figure 56, and by the resource of the particle analysis report function, the area of hairiness is measured. Once the skeleton reduces the width of the fibers to one pixel, the measured area render the length of the fibers, expressed in pixel. The hairiness coefficient is calculated through the division of the measured area by the length of the yarn.

## Experimental Results

This section presents experimental results to demonstrate the application of the determination of yarn production characteristics, diameter and hairiness algorithms showed in the previous sections.

### *Results Yarn Production Characteristics*

This section presents the results obtained with the developed image processing techniques applied to four different cotton linear mass yarns, namely, 62 g/km (Figure 17), 55 g/km (Figure 57), 50 g/km (Figure 58) and 22 g/km (Figure 8).

For the 22 g/km yarn, the image processing application obtained the final image presented in Figure 16. The corresponding particle analysis data is presented in Table 1.

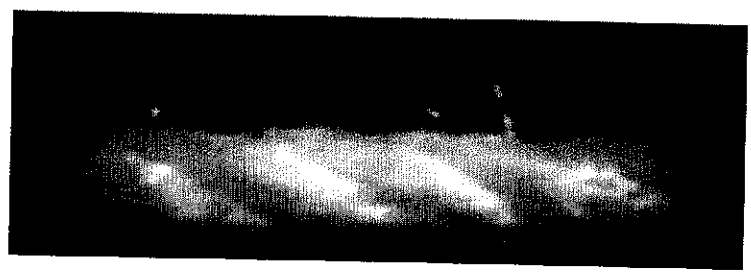

Figure 57. Initial image of the 55 g/km yarn.

Figure 58. Initial image of the 50 g/km yarn.

**Table 1. Results obtained for the 22 g/km yarn**

| Particles | First Horizontal Pixel | Orientation (°) | Area (pixels) |
|---|---|---|---|
| 1 | 52 | 162.9 | 128 |
| 2 | 88 | 168.8 | 145 |
| 3 | 108 | 161.6 | 126 |
| 4 | 140 | 168.0 | 83 |

The average distance between particles together with its standard deviation is 29.3± 8.3 pixels.

Considering the data obtained in Table 1, the following yarn production characteristics were determined:

- Fibers twist orientation: clockwise;
- Folded yarn twist orientation: anti-clockwise;
- Number of cables: more than 1 cable (folded yarn);
- Folded yarn twist step: 0.4±0.1 mm.

Figure 59 shows the final 50 g/km yarn image after image processing while Table 2 displays the particle analysis data obtained.

The distance between the particles is 56.00 pixels. Considering the data obtained in Table 2, the following yarn production characteristics were determined:

- Fibers twist orientation: clockwise;
- Folded yarn twist orientation: anti-clockwise;
- Number of cables: more than 1 cable (folded yarn);
- Folded yarn twist step: 0.77 mm.

Figure 59. Image resulting from the developed application in the 50 g/km yarn.

Figure 60. Image resulting from the application developed in the 55 g/km yarn.

**Table 2. Results obtained for the 50 g/km yarn**

| Particles | First Horizontal Pixel | Orientation (°) | Area (pixels) |
|---|---|---|---|
| 1 | 78 | 160.0 | 156 |
| 2 | 134 | 169.4 | 276 |

**Table 3. Results obtained for the 55 g/km yarn**

| Particles | First Horizontal Pixel | Orientation (°) | Area (pixels) |
|---|---|---|---|
| 1 | 73 | 154.5 | 377 |
| 2 | 116 | 158.0 | 292 |
| 3 | 181 | 174.6 | 120 |

Figure 61. Image resulting from the application developed in the 62 g/km yarn.

**Table 4. Results obtained for the 62 g/km yarn**

| Particles | First Horizontal Pixel | Orientation (°) | Area (pixels) |
|---|---|---|---|
| 1 | 132 | 176.6 | 5527 |

For the 55 g/km yarn, the final image obtained after image processing is presented in Figure 60, while the corresponding particle analysis data is presented in Table 3.

In this case the distance between particles is 54.±15 pixels. Considering the data obtained in table III, the following yarn production characteristics were determined:

- Fibers twist orientation: clockwise;
- Folded yarn twist orientation: anti-clockwise;
- Number of cables: more than 1 cable (folded yarn);
- Folded yarn twist step: 0.7+0.2 mm.

For the 62 g/km yarn, the final image obtained after image processing is shown in Figure 61 and the resulting particle analysis data is listed in Table 4.

As just one particle was detected, this is a single yarn cable and the function of twist orientation described previously in the previous section was activate. A particle orientation angle of 136° was obtained (Figure 61) and the following yarn production characteristics were determined:

- Fibers twist orientation: anti-clockwise;
- Folded yarn twist orientation: not available;
- Number of cables: 1 cable (non folded yarn);
- Folded yarn twist step: not available.

Afterwards, to show that the obtained image processing results are valid and reliable, they were compared with the parameters deduced from detailed electronic microscope

pictures (amplification factor of 40X), for yarns of 50, 55 and 62 g/km, represented in Figure 62 to Figure 64, respectively. Observing Figure 62 and Figure 63 for 50 g/km and 55 g/km yarns, it is verified that these yarns are formed by more than one cable (folded yarns), with a folded yarn twist orientation, anti-clockwise and a fibers twist orientation in the clockwise direction. Considering, Figure 64 (62 g/km), it is verified that this yarn is constituted by a single cable (non folded yarn), with a fibers twist orientation in anti-clockwise direction.

Figure 62. Electron microscope picture of the 50 g/km yarn.

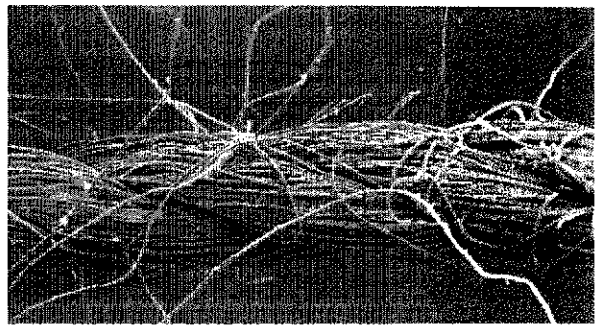

Figure 63. Electron microscope picture of the 55 g/km yarn.

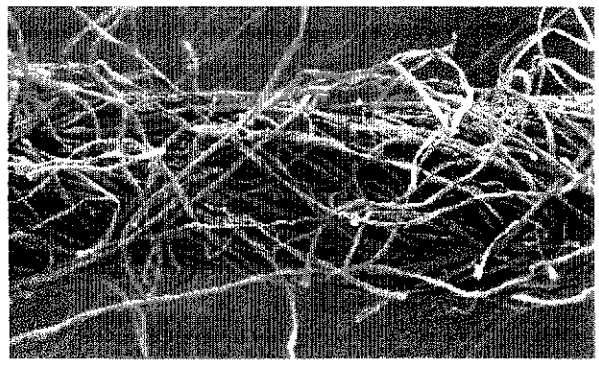

Figure 64. Electron microscope picture of the 62 g/km yarn.

Moreover, a folded yarn twist step between 0.74mm and 0.82mm has been measured over the image for the 50 g/km, and between 0.64mm and 0.78mm, for the 55 g/km yarn. These

results, obtained from the electron microscope images, are in agreement with the results obtained with the developed image processing tool.

This section presents the results obtained with the proposed method for the characterization of the yarn in terms of diameter and hairiness using image processing techniques. It is also performed a comparison between the experimental results of diameter, and the theoretical values of diameter, for different linear masses. Moreover, it is presented a comparison of the hairiness coefficient to the results of the analysis performed using the commercial equipment Uster Tester 3.

***Results Obtained in Diameter Determination***

The algorithm described in the previous section was applied to four sample images with different linear masses (22 g/km, 50 g/km, 55 g/km and 62 g/km) (Figure 65).

Figure 66 presents the images obtained after the application of the image processing techniques to quantify yarn diameter.

Table 5 presents the results in pixels (diameter in pixel – dp) and in real world units (mm) after conversion (diameter experimental – de). It also provides, for a better insight and precision of the algorithm, the values calculated by the theoretical relationship (d(mm)=0.060*sqrt(Tex)) between the yarn mass and the diameter (theoretical diameter - dt) for the respective linear masses.

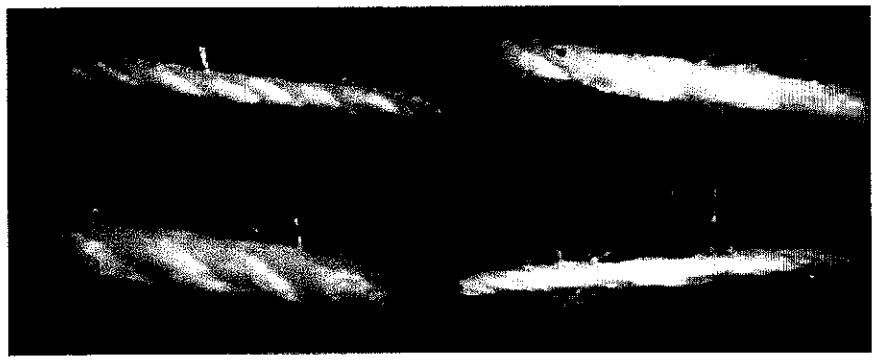

Figure 65. Acquired images a) 22 g/km yarn, b) 50 g/km yarn, c) 55 g/km yarn, c) 16.40 g/km yarn.

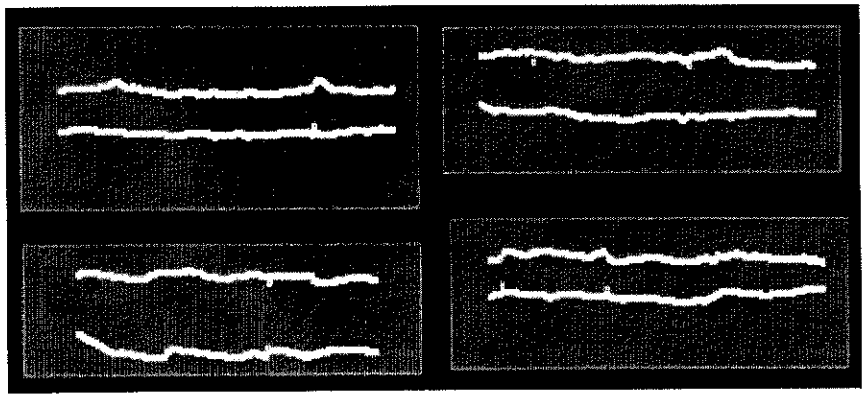

Figure 66. Application of the techniques of image processing to quantify yarn diameter to the images of Figure 65.

**Table 5. Results of the diameter determination**

| Sample Number | Linear Mass (g/km) | dp (pixels) | dt (mm) | de (mm) | Standard Deviation (mm) |
|---|---|---|---|---|---|
| 1 | 22 | 19.65 | 0.2814 | 0.2690 | 0.0086 |
| 2 | 50 | 26.11 | 0.4242 | 0.3576 | 0.0471 |
| 3 | 55 | 32.78 | 0.4449 | 0.4490 | 0.0028 |
| 4 | 16.40 | 17.71 | 0.2429 | 0.2426 | 0.0002 |

***Results Obtained in the Analysis of the Imperfections of the Yarn***

This study was performed through the theoretical correlation between mass and diameter, allowing determining thin places, thick places and neps when comparing the distances detected between the edges, to their average value, allowing identifying yarn imperfections.

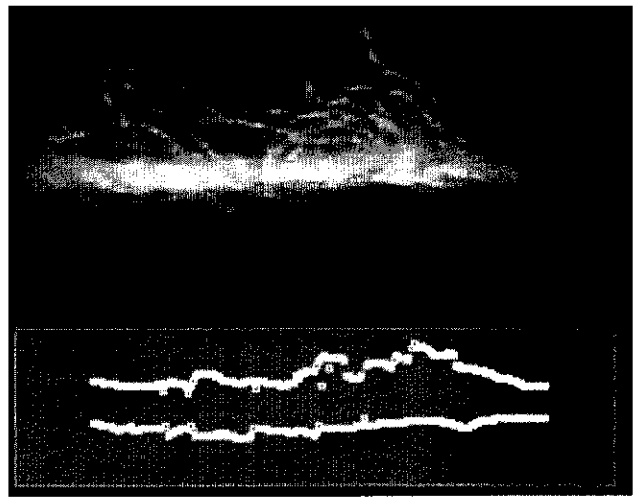

Figure 67. Example of yarn with imperfection.

**Table 6. Yarn faults**

| Sample Number | Thick places | Thin places | Neps |
|---|---|---|---|
| 1 | 0 | 0 | 0 |
| 2 | 0 | 0 | 0 |
| 3 | 2 | 0 | 0 |
| 4 | 0 | 0 | 0 |
| 5 | 0 | 0 | 0 |
| 6 | 2 | 1 | 0 |
| 7 | 4 | 1 | 0 |
| 8 | 0 | 0 | 0 |
| 9 | 0 | 0 | 0 |
| 10 | 2 | 0 | 0 |

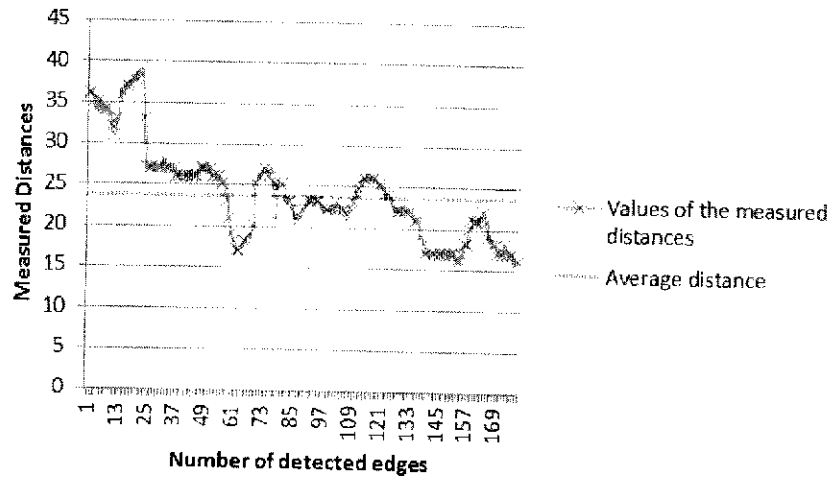


Figure 68. Distances measured over a point on the yarn.

A yarn with linear mass of 19.68 g/km was considered (Figure 67).

Table 6 shows the results of the yarn faults of the 19.68 g/km yarn along the 10 different points.

As it can be observed from Table 6 sample 7 has the higher number of thick places, only in two samples were detected thin places and none neps were detected.

In Figure 68 it can be observed the measured distances over the yarn with linear mass of 19.68 g/km, which corresponds to the sample number 3 of Table 7. By comparing the values with the average distance, clearly notices at least two thick places (distances values between 30 to 40 pixels).

### *Results Obtained in the Hairiness Determination*

It was conducted a comparative test between the proposed approach and the analysis of commercial equipment Uster Tester 3. Five yarns with different linear masses (16.4 g/km to 98g/km) were analyzed, Figure 69.

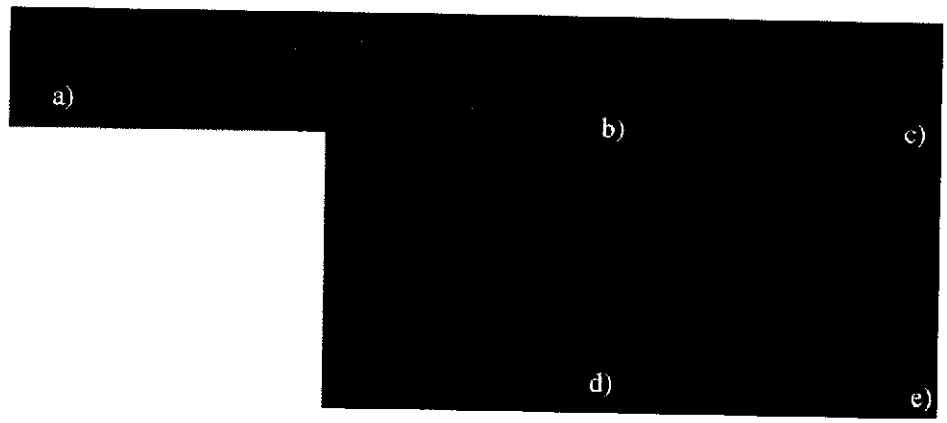


Figure 69. Results obtained for a)16.4 g/km yarn, b)19.68 g/km yarn, c)29.5 g/km yarn, d)36.9 g/km yarn, e)98 g/km yarn.

Figure 70. Example of two different points of the same yarn (19.68 g/km).

**Table 7. Comparison between the average experimental values and the values of Tester 3**

| Sample Number | Linear Mass (g/km) | Vu | Average ve | Relative Error (%) |
|---|---|---|---|---|
| 1 | 16.4 | 4.69 | 4.31 | 8.8 |
| 2 | 19.68 | 7.08 | 6.69 | 5.8 |
| 3 | 29.5 | 4.58 | 6.64 | 31.0 |
| 4 | 36.9 | 4.37 | 4.56 | 4.2 |
| 5 | 98 | 7.18 | 7.15 | 0.4 |
| | | | Average Error: | 10.04% |

In the proposed system, images were acquired at ten different positions of the same yarn sample, Figure 70. This procedure was performed for the five yarns. It was calculated the average values obtained by the new methodology to ones acquired by the commercial equipment.

Table 7 presents the results obtained with the Uster Tester 3 (vu), the average experimental values for different positions of the same yarn obtained by the proposed methodology (ve) and its relative error |((vu-ve/ve)| * 100%). The coefficient of hairiness (v) is given by the ratio between the hairiness lengths and the length of yarn analyzed.

As it can be observed in Table 7 the calculation of the hairiness coefficient from the proposed method is very close to the ones obtained with the commercial equipment validating the approach. A small average error of 10.04% was obtained.

## IMAGE PROCESSING AS A TOOL TO CHARACTERIZE HUMAN BLOOD *SAMPLES*

This section presents the framework, the image processing techniques, the database configuration, the system developed, the statistical analysis and the experimental results of an image processing tool to characterize human blood samples.

## Framework

Determining the blood type of an individual is an essential procedure before administering a blood transfusion, avoiding damage and blood incompatibilities. Thus, the preceding blood test, even in case of medical emergency, is of upmost importance, allowing the administration of the blood type of the receiver in the first unit of blood transfusion. However, although two of the manual tests used in laboratory, the plate test and tube test, allow the analysis in a short time interval, which is suitable for emergency situations, they require travel to the lab and the intervention of a technician, thereby increasing the time spent and the possibility of human error. Given that human errors in the procedure of manual tests, in reading or interpreting the results, can lead to fatal consequences for patients, being one of the significant causes of fatal blood transfusions is extremely important to automate the testing, the reading and the interpretation of results [29-38].

In this sense, various systems were developed, Technicon Auto Analyzer [39-41], Technicon Auto Analyzer II [42, 43], Groupamatic [40, 44], Auto-Grouper [40] Olympus PK 7200 [40, 45-48] Immucor Galileo [49-53], Ortho AutoVue ® Innova System [54], Tango ® Automated Blood Bank [55] and Techno TwinStation [56].

But, none of the systems currently available allow obtaining results on useful time so they can be used in emergency situations [54]. This paper presents an innovative system to automatically perform tests to determine blood type, eliminating human error and in a short interval of time, so they can be used in emergency situations.

This system is based on the plate test for determining blood types and in software developed, using image processing techniques. The plate test consist of the mixture of one drop of blood, and one drop of each reagent, anti-A and anti-B, anti-AB and anti-D, being the result interpreted according to the occurrence or not of agglutination. The agglutination means that a reaction has occurred between the antibody and the cells indicating the presence of the appropriate antigen.

The combination of the occurrence of agglutination, or non-occurrence, determines the blood type of the individual [23]. Thus, the developed software allows, through image techniques, to detect the occurrence of agglutination and consequently the blood type of an individual.

## Image Processing Techniques

The result of the plate test is captured by a CCD camera (Sony Cyber-shot DSC-S750) consisting of a color image composed of four samples of blood and reagent.

This image is processed by image processing techniques developed with the IMAQ Vision software from National Instruments [10]. However, since the original image also needs to be used again at a later stage of processing, it must remain available and unchanged. The following sequences of image processing techniques are used:

1. Image Buffer: Add Copy: This feature allows saving a copy of the original color image captured by the CCD camera after performing the test procedure for determining the blood type. It is the first function to be used as it is necessary to keep the original image intact, i.e. before undergoing transformations carried out by other

image processing functions. The image is stored in Buffer # 1 and is available for later use [10, 11]. The result of applying

This function is shown in Figure 71, for the four reagents, anti-A and anti-B, anti-AB and anti-D.

2. Color Plane Extraction: RGB Green Plane: This function is used to extracting green plans in a RGB image, allowing transforming the original color image composed of 32 bit in a grayscale image of 8 bit. This step is essential in order to use functions like threshold that can only be applied to binary images or images with 8 bit, 16 bit or float [10, 11]. The image obtained by applying this function to the image of Figure 72 is shown in Figure 71.

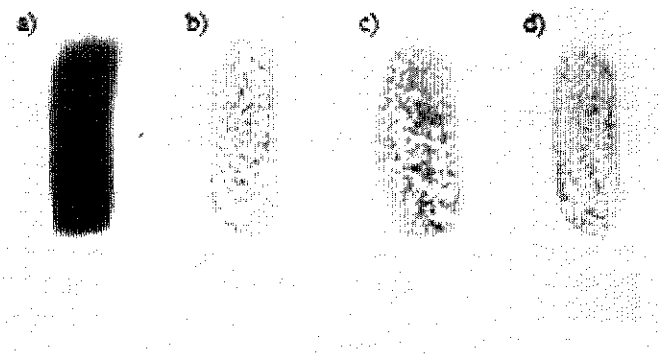


Figure 71. Original image captured by the CCD camera (a) Reagent Anti-A (b) Reagent anti-B (c) Reagent anti-AB (d) Reagent anti-D.

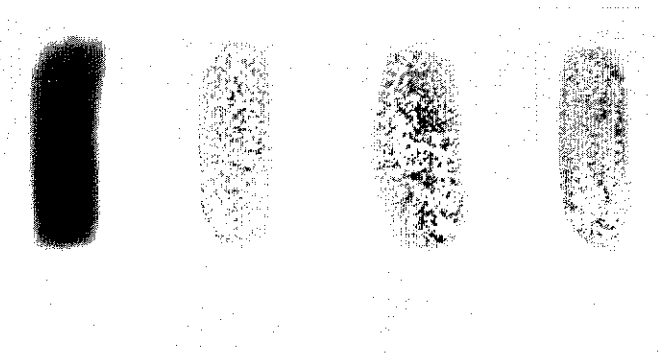

Figure 72. Image obtained by applying Color Plane Extraction: RGB Green Plan function in the original image of Figure 71.

3. Auto Threshold: Clustering: This function applies a threshold based on a statistical technique called clustering and it is used to separate the blood samples and reagent into two regions, designated "particle region" and "background region". This process is accomplished by changing all pixels that lie between the range of values

established (designated threshold range) changing all other image pixels to 0 [10, 11]. Thus, to isolate the particles of interest and convert the gray scale image (pixel values between 0 and 255) into a binary image (pixel values of 1 and 0). This function is an automatic threshold, as it is not necessary to specify the minimum and maximum light intensity. To draw the threshold, it is used the image histogram [10, 11]. The image obtained with the application of this function is shown in Figure 73.

Now that the particles of interest are separated from the background of the image, it is necessary to isolate the four particle image and eliminate any unwanted particles. So, there were used the following three functions, Local Threshold: Niblack, Advanced Morphology: Fill holes and Advanced Morphology: Remove small objects.

4. Local threshold: Niblack: In this function the threshold value for each pixel is calculated based on statistics from adjacent pixels. It uses a kernel, by default, of 32 width and 32 height, with a deviation factor which by default is 0.20 [10, 11]. This function is extremely important to isolate the particles to be analyzed. The result of applying this function on the image of Figure 73 can be seen in Figure 74.
5. Advanced Morphology: Fill holes: This function fills all the holes that are present inside the particles with a pixel of value 1. The binary image resulting from the application of this function contains particles intact, without holes, corresponding to samples of blood and reagent [10, 11]. The result of applying this function is presented in Figure 75.

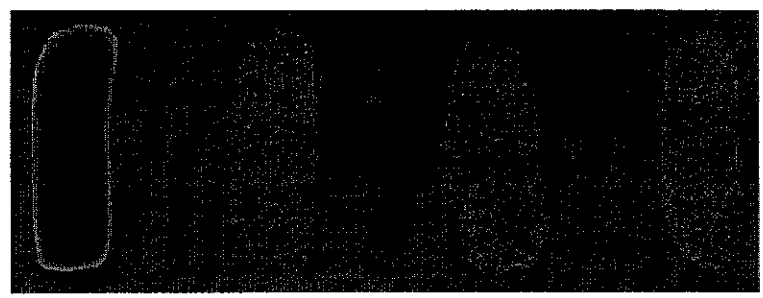

Figure 73. Image obtained by applying the Auto Threshold: Clustering in the image of Figure 72.

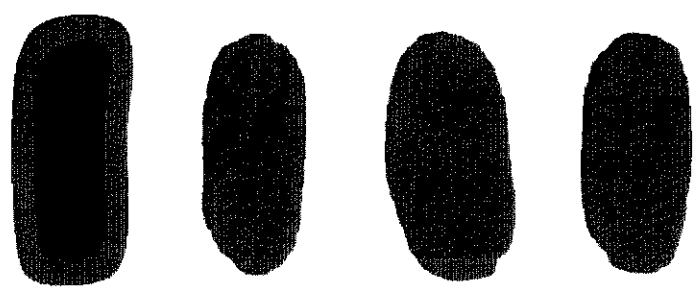

Figure 74. Image obtained by applying the Local Threshold: Niblack function under the image of Figure 73.

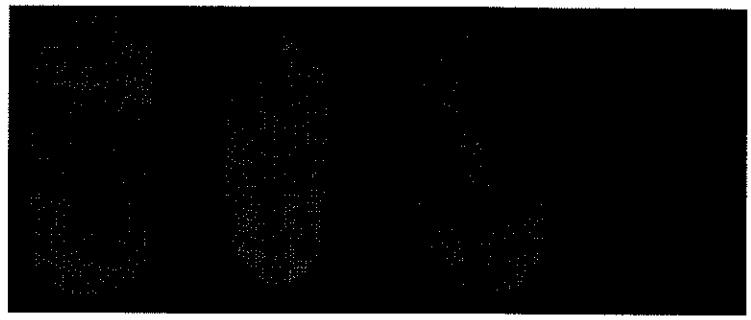

Figure 75. Image resulting from the application of Advanced Function Morphology: Fill holes function in the image of Figure 74.

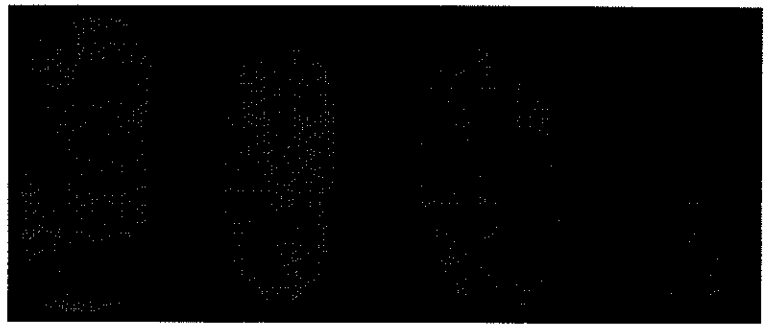

Figure 76. Image resulting from the application of Advanced Function Morphology: Remove small objects in the image of Figure 75.

- Advanced Morphology: Remove small objects: This function uses a low pass filter to remove small particles and the possible noise in the binary image resulting from the previous function. The particles are removed according to their widths, as defined by a specific parameter, filter size. Thus, for a given filter size N, the low pass filter removes the particles whose widths are less than or equal to (N-1) pixels. These particles disappear after (N-1) / 2 erosions [10, 11]. The function removes particles that are not relevant to the analysis, leaving the rest of the particles (larger particles) untouchable. The particles that are removed from the step of erosion particles are assumed to be noise. It is mainly used to remove particles that may interfere with the analysis of the image, like little drops of blood or reagent at the background of the image [10, 11]. The result of this function is presented in Figure 76.

In this case, as there are only very small particles in Figure 75, which are difficult to see [illegible] the application of this function is not noticeable in Figure 76.

However, when there are small drops of liquid (blood or reagent) present in the image, it [illegible] crucial to use this function to remove the unwanted particles.

The functions presented at this stage are essential for the automation of the process of [illegible] the blood type.

- Particle Analysis: A particle is a continuous group of nonzero values in an image. The particles can be characterized by measures related to their attributes such as

location of particles, area, and shape, among others. Therefore, this step is used to analyze the properties of particles in the image, considered as four particles corresponding to each of the mixtures of blood and reagent. These particles can be analyzed using various properties, being the center of mass highly important in this work. The result of this function is a table that contains all the selected properties and their values for each of the particles. The values of the center of mass X (coordinate X of the center of mass) and the center of mass Y (coordinate Y of the center of mass) for each particle are shown in Table 8.

**Table 8. Results of Application of Particle Analysis Function on image of Figure 75**

| Particle | Center of Mass X | Center of Mass Y |
|---|---|---|
| 1 | 338,48 | 537,65 |
| 2 | 1163,82 | 557,58 |
| 3 | 735,68 | 545,93 |
| 4 | 1570,67 | 545,81 |

2. Image Buffer: Retrieve Buffer # 1: This function retrieves a copy of the original color image stored in Buffer # 1, so it can be used in the next function. The original image consists of four samples of blood and reagents that will be processed and analyzed to detect the occurrence of agglutination [10, 11].The original image, as previously referred, is shown in Figure 71.
3. Color Plane Extraction: HSL Luminance Plane: This function is used to extract the planes of a color image light obtained with the previous function [10, 11] and allows transforming the original image constituted of 32 bit in a grayscale image constituted of 8 bit. Thus, it makes possible the use of the Quantify function that can only be applied to images of binary type, or images with 8-bit and 16 bit float, or grayscale images. The image obtained by applying this function to the image of Figure 71 is shown in Figure 77.
4. Set Coordinate System: This function defines a coordinate system based on the stage of particle analysis. The function of particle analysis obtains the coordinates (center of mass X and center of mass Y) needed to calculate the center of mass used in this function. This function is essential because it is based on the coordinate system, which is selected to analyze the region, depending on the center of mass calculated in the step of particle analysis. Thus, the selection process in the region of interest analysis is automatic and depends on the center of mass of each particle. This step is repeated for each of the particles to be analyzed. In this case it will be repeated four times, one for each sample of blood and reagent [29-31]. The image obtained by applying this function to each particle image is shown in Figure 78.
5. Quantify: This function can measure the intensity of pixels in the region of interest selected. This step uses the options, Reposition Region of Interest and Reference Coordinate System. The first option, Reposition Region of Interest, dynamically restores the region of interest based on the coordinate system previously defined. The second option, Reference Coordinate System, allows to select the coordinate system associated to the region of interest. The analysis of each sample is automatically

performed. The result of this function is a table that contains the area (percentage of surface examined for the full image), the mean (average value of pixels), standard deviation (standard deviation of pixels), the minimum and maximum value of pixels intensity. Using this feature, it allows identifying the occurrence of agglutination in the blood sample and reagent based on the value of standard deviation. As in the previous function, this step is repeated for each of the particles to be analyzed [10, 11]. The image obtained by applying this function is shown in Figure 79 and the resulting table is shown in Table 9.

The value of standard deviation is essential to detect the occurrence of agglutination. In samples where no agglutination occurs, the values of standard deviation do not exceed 16, taken normally, values between 0 and 10. Moreover, samples where agglutination occurs show standard deviation values greater than or equal to 16, showing even high standard deviation values between 20 and 70.

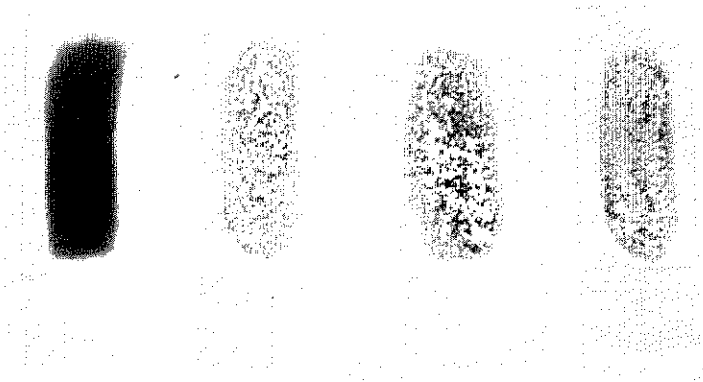

Figure 77. Image obtained by applying the Color Plane Extraction: HSL Luminance Plane function to the original image of Figure 71.

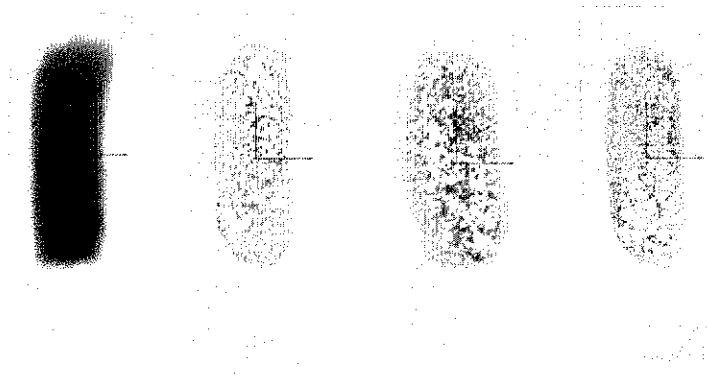

Figure 78. Image resulting of the application of Set Coordinate System functions to each of the particles in the image.

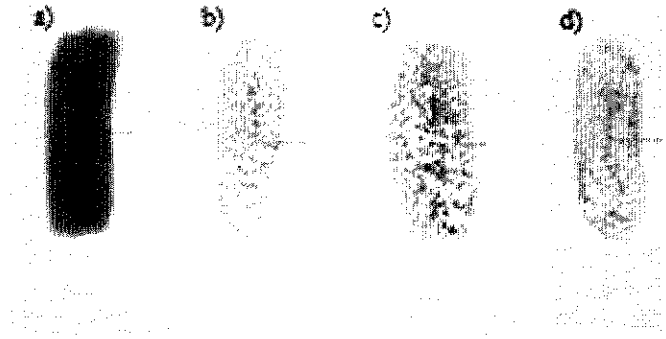


Figure 79. Image resulting from the application of the Quantify function.

**Table 9. Results of Application of the Quantify Function in Figure 78**

| Fig. | Area | Mean Value | Standard Deviation | Minimal Value | Maximal Value |
|---|---|---|---|---|---|
| 79 (a) | 0.5 | 57.6 | 5.2 | 43.0 | 83.0 |
| 79 (b) | 0.4 | 193.5 | 43.7 | 63.0 | 250.0 |
| 79 (c) | 0.5 | 176.9 | 53.4 | 46.0 | 248.0 |
| 79 (d) | 0.4 | 182.9 | 25.5 | 61.0 | 234.0 |

Thus, it was established as a threshold value for classification, a standard deviation of 16; samples with a standard deviation value below 16 are classified as samples with no agglutination and samples with a standard deviation value greater than or equal to 16 are classified as samples in which agglutination occurred. Having verified the occurrence of agglutination in anti-B reagent, anti-AB and anti-D, it is confirmed the presence of B antigens and Rh antigens in the blood sample analyzed. Thus, it can be concluded that the blood type in question is B Positive. Another example of the application of the methodology described is presented in Figure 80, where agglutination occurred in samples a), c) and d); in sample b), there was no agglutination. Through the standard deviation values of Table 10, this is also confirmed as samples a), c), d), present values of standard deviation of 57.8, 62.1 and 49.5 respectively (all above 16), sample b), obtained 3.4 (below 16).

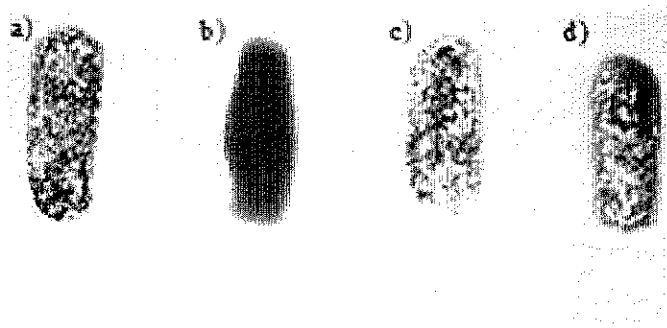


Figure 80. The original image of A Positive (a) Reagent Anti-A (b) Reagent anti-B (c) Reagent anti AB (d) Reagent anti-D.

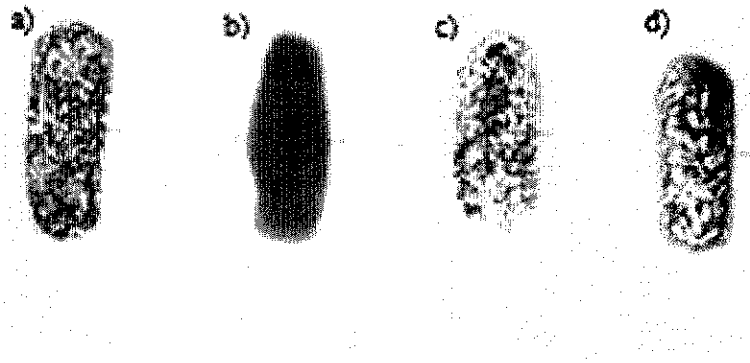


Figure 81. Image resulting from application of image processing techniques presented to the image of Figure 80.

**Table 10. Results of Application of Quantify Function on image of Figure 81**

| Fig. | Area | Mean Value | Standard Deviation | Minimal Value | Maximal Value |
|---|---|---|---|---|---|
| 81 (a) | 0.5 | 144.3 | 57.8 | 20.0 | 238.0 |
| 81 (b) | 0.5 | 83.4 | 3.4 | 64.0 | 95.0 |
| 81 (c) | 0.4 | 147.4 | 62.1 | 32.0 | 240.0 |
| 81 (d) | 0.4 | 139.3 | 49.5 | 34.0 | 222.0 |

Having verified the occurrence of agglutination in anti-A reagent, anti-AB and anti-D, it is confirmed the presence of A antigens and Rh antigens in the blood sample analyzed. Thus, it can be concluded that the blood type in question is A Positive.

## Database

To store the information from the analysis of detection of agglutination performed through the techniques of image processing and the result of the classification algorithm developed to determine blood type, it was designed and implemented a database. This section presents the table of the database developed with Microsoft Office Access 2007, where information will be stored, Figure 82.

This table, Figure 82, stores the image captured and used in image processing (each image contains four samples of blood and reagents), the standard deviation calculated in each sample image, the occurrence or not of agglutination and the blood type.

## System Developed

This section presents on one hand the software developed taking into consideration the studies performed in the previous sections and on the other hand the first prototype of the acquisition hardware designed.

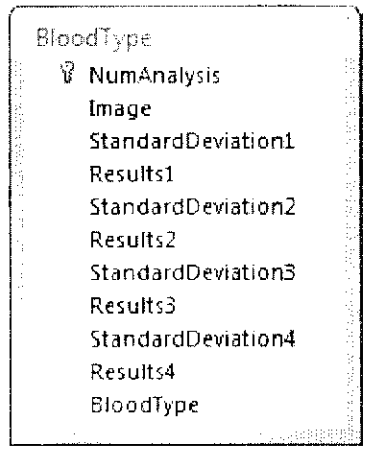


Figure 82. Base table where the information is entered.

### *Software Developed*

The software was developed in LabIEW from National Instruments [10, 11].The front panel is shown in Figure 83.

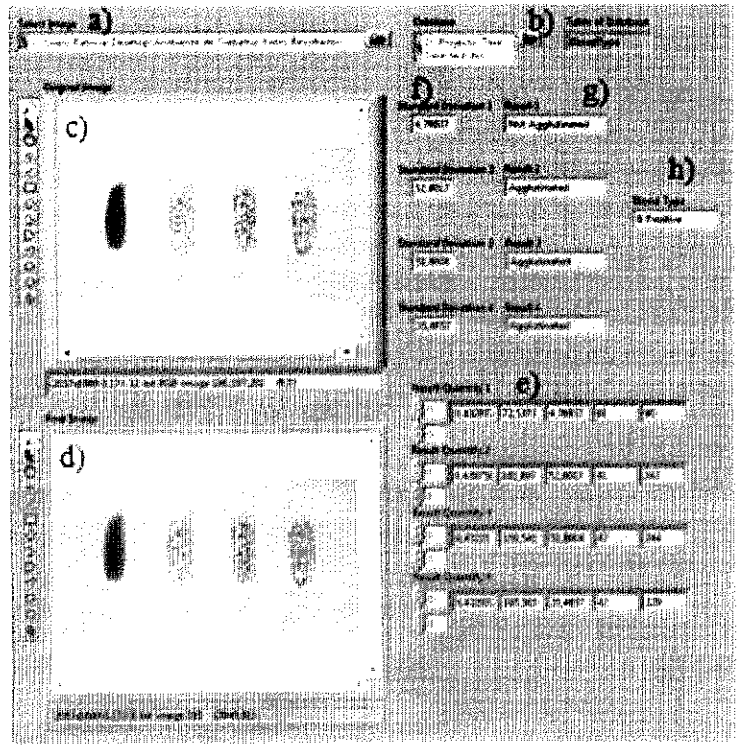


Figure 83. Developed Software. (a) Selection of the image (b) Selection of File Database.dsn and entering the name of the table of database (c) Original Image (d) Final image obtained with the image processing techniques (e) Results of the Quantify function (f) Values of standard deviation of each sample (g) Results based on the standard deviation of each sample (h) Result of the classification algorithm.

This software allows to select the image to be used, Figure 83(a), the database to establish a connection and the table from the database where information is added to the analysis, Figure 83(b), it displays the original image that is being used, Figure 83(c) as well as the final image obtained with the image processing techniques, Figure 83(d), it shows the results of the Quantify function, Figure 83(e), the results of the standard deviation, Figure 83(f), the results based on standard deviation values calculated Figure 83(g), and, finally, the result in terms of blood type, Figure 83(h).

### *Hardware Developed*

The first prototype of the developed system, which automatically determines the blood type of an individual, using as reference the plate test [28], is shown in Figure 84.

The system requires that the blood samples and the reagents are manually placed, in plates, by the user. It is placed on the first plate the reagent anti-A, on the second plate the reagent anti-B, on the third plate the reagent anti-AB and on the fourth plate the reagent anti-D. Thereafter, the system moves the plates for the mixing area, where the blood and the reagents in each plate, are mixed. This mixture is performed with a DC motor and without contamination between the four samples. Upon completion of the mixing, blades are moved to the image capture area, where a motor drives the webcam Glossy, 5 Mega pixels, along the samples, capturing an image from each of the plates.

These images are stored for later analysis. The system is controlled by the microcontroller Arduino. Some of its characteristics are 14 digital I/O, 6 analog inputs, 16KB of flash memory, 512 bytes of SRAM, 512 bytes of EEPROM and a clock speed of 16 MHz.

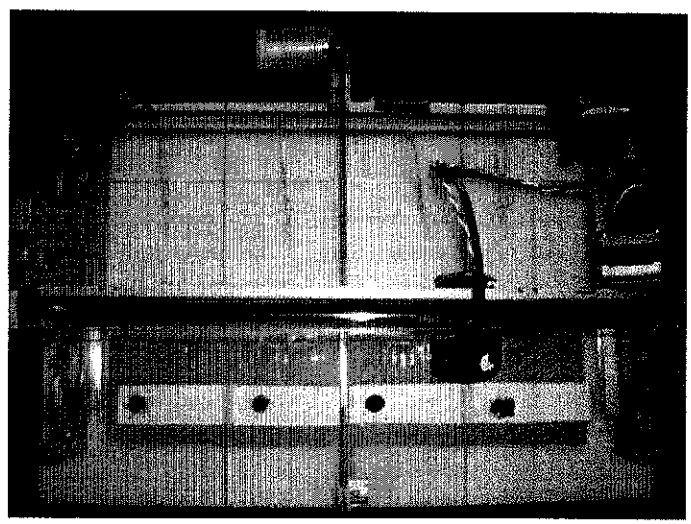

Figure 84. System Developed – first prototype.

## Statistical Analysis

This section presents the statistical analysis used to prove that the boundary between the occurrence of agglutination and non-agglutination is reliable.

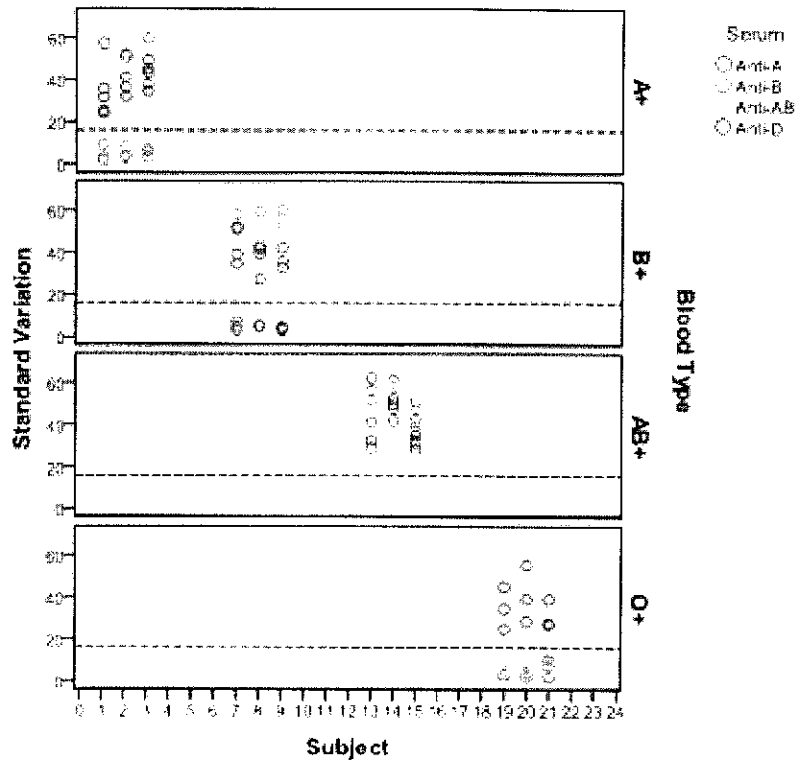


Figure 85. Standard deviation values obtained by the image processing techniques, for all individuals Rh Positive (D Positive).

Namely, there are no values of agglutinated samples below the limit (16) and there are no values upper the limit (16) for samples that are not agglutinated.

This statistical analysis allows determining the reliability of the methodology used as well as the limit set on the basis of the statistical tests.

To this end, tests were performed on determining blood type of 24 individuals, using the software developed in this work. For each individual, the procedure for determining the blood type was repeated three times in order to verify whether the results were similar. There were obtained a total of 288 results for analysis.

It is noteworthy that the blood type of the tested individuals was previously determined by the technique of determining the blood type currently used in laboratories, Cards-ID [23] in order to verify the validity of the technique developed in this work.

The results of statistical analysis were obtained using SPSS software (Version 17.0) [57], being the standard deviation value used to analyze the reliability of the technique. The statistical analysis was based on descriptive data analysis. The study of the variability for each blood type results is shown in Figure 85 and Figure 86.

The study of variability was performed, initially for individuals Rh positive and at a second stage, for individuals Rh Negative. The dashed line represents the limit of standard deviation, 16, set out to determine the occurrence or non-occurrence of agglutination. For all samples, there were no standard deviation values that could lead to wrong decisions. For example, in case of blood type A+ (A Positive), agglutination was not observed for the reagent anti-B in all tests (Figure 85, green).

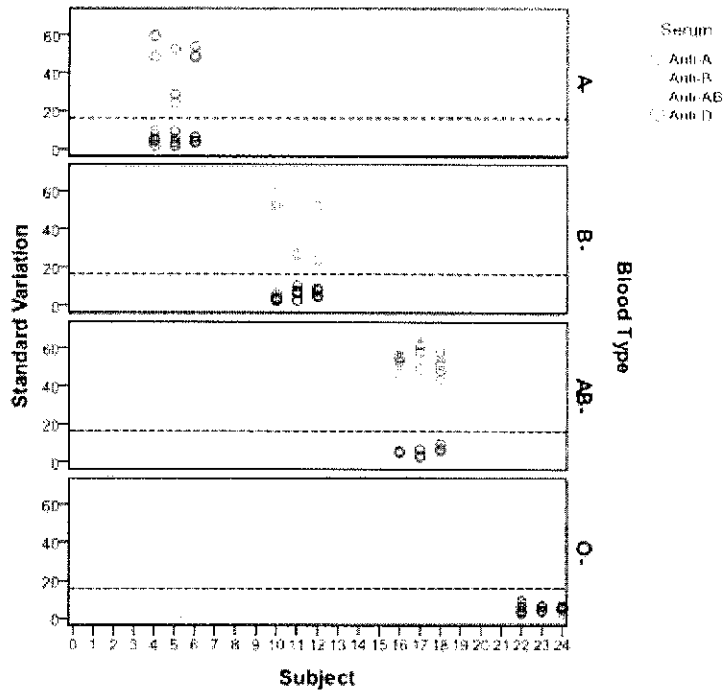


Figure 86. Standard deviation values obtained by the image processing techniques, for all individuals Rh Negative (D Negative).

For this case, all standard deviation values obtained are below the threshold. For the case of blood type O-(O Negative), agglutination does not occur in all reagents and in all tests, all standard deviation values obtained are below 16 (Figure 86). On the other hand, for blood type AB+ (AB Positive), all values are higher than 16 (Figure 85).

For each test the agglutination was detected always getting standard deviation values higher than or equal to 16. The same was true for the absence of agglutination, obtaining values of standard deviation always below 16.

## Conclusion

### Textile Industry Application

Regarding the results obtained for each of the parameterization performed (yarn production characteristics, yarn diameter and imperfections and yarn hairiness determination) it can be concluded that its reliability allows to take into consideration the option of use an image processing system instead of a traditional system based on capacitive and optical sensors. Apart from other benefits, its low cost, portability and reduced maintenance give proper indicators in order to justify its adoption to offline yarn analysis systems. Moreover, and with the prospect of continuing this project, among other developments, it is suggested improving the methods to detect and distinguish between the loop and protruding fibers supported by artificial intelligence algorithms. As for the methodologies developed there is still the possibility to test them in different types of yarns, such as fancy yarns.

## Biomedicine Application

The methodology used in this work (previously validated by conventional methods) is capable to determinate blood types safely and in a short time (approximately 2 minutes) allowing it to be used in emergency situations. As demonstrated, the techniques applied are able to detect the agglutination (using a standard deviation value of 16 as threshold), and consequently blood types. The equipment developed is able to determine blood types using the plate test and to automatically perform the analysis, with exception to the introducing of blood and reagents that at this stage of development is performed manually. For future work, it is intended to evolve the system, reducing its size, automate all the processes and incorporate GSM technology, among other features.

## References

[1] M. Kuzanski and L. Jackowska-Strumillo,Yarn Hairiness Determination – The algorithms of computer measurement methods. MEMSTECH'2007, May 23-26, Lviv-Polyana, Ukraine, p.154-157.

[2] M. Kuzanski, Measurement Methods for Yarn Hairiness Analysis – the idea and construction of research standing. MEMSTECH'2006, May 24-27, Lviv-Polyana, Ukraine, p.87-90.

[3] Shiloh, M., A computer for the evaluation of the crimp diameter of textile fibers. *Textile Research Journal*, 1964, 34(5): p. 430-434.

[4] S. Jaganathan, Characterization Methods and Physical Properties of Novelty Yarn. MSc Thesis, North Carolina State University, Raleigh, 2005.

[5] Anirban Guha, C. Amarenath, S. Pateria and R, Measurement of yarn hairiness by digital image processing. *The journal of the Textile Institute*, Vol. 101, Issue 3, March 2010, pp. 214-222.

[6] http://www.indiantextilejournal.com/articles/FAdetails.asp?id=552 (access in March 2011).

[7] M. Kuzanski, The Algorithms of the Yarn Shape Detection and Calculation of the Protruding Fibres Length. MEMSTECH'2008, May 21-24, Lviv-Polyana, Ukraine, p.98-100.

[8] W. Jian and Y. Li, Evaluation of Yarn Regularity Using Computer Vision. *9th International Conference on Pattern Recognition*, Vol. 2, November 14-17, p.854-856.

[9] V. Carvalho, Automatic Yarn Characterization System. PhD Thesis, Minho University, Braga, 2008.

[10] IMAQ, IMAQ Vision Concepts Manual. *National Instruments*, Austin, 2004.

[11] C. Relf, Image Acquisition and Processing with LabVIEW. CRC, Boca Raton, 2003.

[12] N. Gonçalves, V. Carvalho, F. Soares, Rosa Vasconcelos and Michael Belsley, Yarn mass parameters determination using Image Processing techniques. CMNE 2011, Coimbra, Portugal, 11-17 June.

[13] V. Carvalho , F. Soares, Rosa Vasconcelos, Michael Belsley and N. Gonçalves, Yarn hairiness determination using Image Processing techniques. ETFA 2011, Toulouse, France, 21-27 August 2011.

[14] V. Carvalho, M. Belsley, R. Vasconcelos and F. O. Soares, Determination of Yarn Production Characteristics Using Image Processing. (*International Journal of Imaging Systems and Technology*, Vol. 20, November 2010, pp. 391-399).
[15] N. Gonçalves, Parametrização de Fio Têxtil Baseada em Técnicas de Processamento de Imagem. Msc. Thesis, Minho University, Braga 2010 (in portuguese)
[16] Ferraz, V. Carvalho, F.Soares and C.P. Leão, Characterization of Blood Samples Using Image Processing Techniques. Sensors and Actuators A. published online in 25th, February 2011, doi: 10.1016/j.sna.2011.02.022.
[17] Ferraz , V. Carvalho and P. Brandão, Automatic Determination of Human Blood Types using Image Processing Techniques. BIODEVICES 2010, 20-23 January 2010, Valencia, Spain).
[18] Ferraz, V. Carvalho and F. Soares, Development of Human Blood Type Detection Automatic System. EUROSENSORS 2010, 5-8 September, 2010, Linz, Austria.
[19] Ferraz, V. Moreira, D. Silva, V. Carvalho and F. Soares, Automatic system for blood type classification using image processing techniques. *BIODEVICES* 2011, Rome, Italy, 26-29 January, 2011.
[20] Ferraz V. Moreira, V. Carvalho and F. Soares, Automatic system of human blood types determination. 1° Encontro Nacional de Bioengenharia, Lisbon, Portugal IST, 1-4 March 2011.
[21] M. R. Brown, P. Crim., Organizing the antibody identification process. *Clin. Lab. Sci.*, vol. 20, 2007, pp. 122–126.
[22] A. Myhre and D. McRuer, Human error – a significant cause of transfusion mortality. *Transfusion*, vol. 40, Jul. 2000, pp. 879–885.
[23] Datasheet of Diamed-ID Micro Typing System, Card-ID. Diaclon ABO\Rh for patients. Cressier, 2008.
[24] R. Furter, Evenness Testing in Yarn Production: part I, The Textile Institute and Zellweger Uster AG, Manchester: 1982.
[25] M. Castro and M. Araújo, Manual de Engenharia Têxtil - Vol. II, Gulbenkian, Lisbon, 1986.
[26] Goswami, J. Martindale and F. Scardino, Textile Yarns: Technology, Structure and Applications, 2nd Edition, John Wiley and Sons, New York, 1977.
[27] http://www.bresseroptics.co.uk (access in March 2011).
[28] http://www.hercules.com (access in March 2011).
[29] M. R. Brown and P. Crim. Organizing the antibody identification process. *Clin. Lab. Sci.*, vol. 20, 2007, pp. 122–126.
[30] A. Myhre and D. McRuer, Human error – a significant cause of transfusion mortality. *Transfusion*, vol. 40, Jul. 2000, pp. 879–885.
[31] I. Petaja, S. Andersson and M. Syrjala, A simple automatized audit system for following and managing practices of platelet and plasma transfusions in a neonatal intensive care unit. *Transfus Med.*, vol. 14, 2004, pp. 281–288.
[32] M. Delamaire, Automation of the immunohematology laboratory. *Transfus Clin. Biol.*, vol. 12, 2005, pp. 163–168.
[33] A. Henneman, G. S. Avrunin, L. A. Clarke, L. J. Osterweil, C. Jr. Andrzejewski, K. Merrigan, R. Cobleigh, K. Frederick, E. Katz-Bassett and P. L. Henneman, Increasing patient safety and efficiency in transfusion therapy using formal process definitions. *Transfus Med. Rev.*, vol. 21, 2007, pp. 49–57.

[34] A. Wagar, L. Tamashiro, B. Yasin, L. Hilborne and D. A. Bruckner, Patient safety in the clinical laboratory: a longitudinal analysis of specimen identification errors. *Arch. Pathol. Lab. Med.*, vol. 130, 2006, pp. 1662–1668.

[35] L. Turner, A. C. Casbard and M. F. Murphy, Barcode technology: its role in increasing the safety of blood transfusion. *Transfusion*, vol. 43, 2003, pp. 1200–1209.

[36] J. L. Callum, H. S. Kaplan, L. L. Merkley, P. H. Pinkerton, B. R. Fastman, R. A. Romans, A. S. Coovadia and M. D. Reis, Reporting of near-miss events for transfusion medicine: improving transfusion safety. *Transfusion*, vol. 41, 2001, pp. 1204–1211.

[37] M. M. Mueller and E. Seifried, Blood transfusion in Europe: basic principles for initial and continuous training in transfusion medicine: an approach to an European harmonization. *Transfus Clin. Biol.*, vol. 13, 2006, pp. 282–285.

[38] Stainsby, H. Jones, D. Asher, C. Atterbury, A. Boncinelli, L. Brant, C. E. Chapman, K. Davison, R. Gerrard, A. Gray, S. Knowles, E. M. Love, C. Milkins, D. B. McClelland, D. R. Norfolk, K. Soldan, C. Taylor, J. Revill, L. M. Williamson and H. Cohen. for the SHOT Steering Group, Serious hazards of transfusion: a decade of hemovigilance in the UK. *Transfus Med. Rev.*, vol. 20, 2006, pp. 273–282.

[39] "Blood Policy and technology", Congress, Office of Technology Assessment, Washington, DC: U.S. January 1985. Available: FAS http://www.fas.org/ota/reports/8505.pdf.

[40] P. Sturgeon, Automation: its introduction to the field of blood group serology. *Immunohematology Journal of Blood Group Serology and Education*, vol. 17, no. 4, 2001.

[41] W. A. Coakly, Handbook of Automated Analysis. Mercel Dekker, 1981 pp. 61.

[42] W. Ewing, Analytical Instrumentation Handbook. 2nd ed., Ed. New York: Marcel Dekker, pp.152.

[43] AutoAnalyzerhttp://weather.nmsu.edu/Teaching_Material/soil698/Student_Material/Autoanalyzer/Autodiag.html (accessed in July 2010).

[44] M. Garretta, J. Gener, A. Muller, C. Matte and J. Moullec, The Groupamatic System for Routine Immunohematology. Transfusion, vol. 15, Sep.-Oct. 1975, pp. 422-431.

[45] Zaccarelli, G. Monti, J. Malaguti, D. Marchesini, F. Figliola, G. Cagliari, C. basile and P. Zucchelli, Esperienza di automazione nella determinazione dei gruppi sanguigni. La Transfusione del Sangue, vol. 45, no. 1, gennaio – febbraio 2000.

[46] Olympus http://www.olympus-global.com/en/magazine/techzone/vol67_ e/page5.cfm (accessed in July 2010).

[47] Fuji http://www.mastgrp.com/Fuji/IFU/TPPAauto.pdf (accessed in July 2010).

[48] Olympus, Formulated for use in Automated System Olympus® PK® Systems. December 2007.

[49] Immucorhttp://immucor.com/site/aum_company_profile.jsp (accessed in July 2010).

[50] Wittmann, J. Frank, W. Schram and M. Spannagl., Automation and Data Processing with the Immucor Galileo® System in a University Blood Bank. *Transfusion Medicine Hemotherapy*. vol. 34, pp. 347-352. Available: Kargerwww.karger.com/tmh (2007)

[51] Briefingresearchhttp://www.briefingresearch.com/GeneralContent/Investor/Active/ArticlePopup/ArticlePopup.aspx?SiteName=InvestorPopUpandArticleId=NS20070619155112AheadOfTheCurve (accessed in July 2010).

[52] Stanford http://securities.stanford.edu/1035/BLUD05_01/200622_r01c_0502276.pdf (accessed in July 2010).

[53] Biologichttp://www.fda.gov/downloads/BiologicsBloodVaccines/BloodBloodProducts/ApprovedProducts/LicensedProductsBLAs/BloodDonorScreening/BloodGroupingReagent/ucm080763.pdf (accessed in July 2010).

[54] Dada, D. Beck and G. Schmitz., Automation and Data Processing in Blood Banking Using the Ortho AutoVue® Innova System. *Transfusion Medicine Hemotherapy*, vol. 34, pp. 341–346. Available: Kargerwww.karger.com/tmh, (2007).

[55] S. Y. Shin, K. C. Kwon, S. H. koo, J. W. Park, C. S. Ko, J. H. Song, and J. Y. Sung, Evaluation of two automated instruments for pre-transfusion testing: AutoVueInnova and Techno TwinStation, *Korean J. Lab. Med.*, vol. 3, Jun. 2008. pp. 214-220.

[56] Dada, D. Beck and G. Schmitz. (2007), Automation and Data Processing in Blood Banking Using the Ortho AutoVue® Innova System. Transfusion Medicine Hemotherapy, vol. 34, pp. 341–346. Available: Kargerwww.karger.com/tmh.

[57] SPSS 17.0, SPSS http://www.spss.com/ (accessed in July 2010).